A Galerkin-characteristic unified finite element method for moving thermal fronts in porous media

Loubna Salhi[a,*], Mofdi El-Amrani[b], Mohammed Seaid[c,d]

[a]*Laboratory of Complex Systems Engineering & Human Systems, University Mohammed VI Polytechnic, Benguerir, Morocco*

[b]*Dpto. Matemáticas Applicada, Ciencia e Ingeniería de Materiales y Tecnología Electrónica, Universidad Rey Juan Carlos, 28933 Móstoles-Madrid, Spain*

[c]*Department of Engineering, University of Durham, South Road, DH1 3LE, UK*

[d]*International Water Research Institute, University Mohammed VI Polytechnic, Benguerir, Morocco*

Abstract

We investigate the performance of a unified finite element method for the numerical solution of moving fronts in porous media under non-isothermal flow conditions. The governing equations consist of coupling the Darcy equation for the pressure to two convection-diffusion-reaction equations for the temperature and depth of conversion. The aim is to develop a non-oscillatory unified Galerkin-characteristic method for efficient simulation of moving fronts in porous media. The method is based on combining the modified method of characteristics with a Galerkin finite element discretization of the governing equations. The main feature of the proposed unified finite element method is that the same finite element space is used for all solutions to the problem including the pressure, velocity, temperature and concentration. Analysis of convergence and stability is also presented in this study and error estimates in the L^2-norm are established for the numerical solutions. In addition, due to the Lagrangian treatment of convection terms, the standard Courant-Friedrichs-Lewy condition is relaxed and the time truncation errors are reduced in the diffusion-reaction part. We verify the method for the benchmark problem of moving fronts around an array of cylinders. The numerical results obtained demonstrate the ability of the proposed method to capture the main flow features.

Keywords: Moving fronts, Darcy flow, Porous media, Galerkin-characteristic method, Unified finite elements, A priori error estimates.

1. Introduction

Moving fronts in porous media occur in many engineering applications including combustion and carbon dioxide storage [1, 2, 3]. The focus in these problems is mainly on moving fronts produced by the thermal frontal polymerizations. In this case, the chemical reactions are a process in which liquid monomers are converted into polymers via a localized and specific reaction zone, thus generating the so-called polymerization front which propagates through the medium if the reaction is exothermic and highly activated. Frontal polymerization has a variety of possible uses including material synthesis, curing large composites, filled materials, microfluidic applications, and determining whether some systems obey the Snell's law of refraction [4]. Its advantages in different combustion systems include the ability to vary the morphology, lower energy consumption, and rapid conversion of monomers to polymers [5]. In many applications, frontal polymerization processes are exothermal reactions that produce an important heat removal which may lead to possible heat explosion and reduction of the reagent concentration. In general injection of a reactive fluid into a porous medium leads to alteration of the reactive part and to changes in the porosity and

*Corresponding author

Email addresses: `loubna.salhi@um6p.ma` (Loubna Salhi), `mofdi.elamrani@urjc.es` (Mofdi El-Amrani), `m.seaid@durham.ac.uk` (Mohammed Seaid)

permeability of the medium. Under certain conditions of flow and reaction, the alteration pattern becomes a reaction front. The front is a transition from fully reacted to unreacted rock over a narrow reaction zone. The reactive part of the matrix has fully reacted behind the front and it is unreacted ahead of the front. The effect of natural convection on the heat transfer was first studied in [6, 7]. It was shown that the critical value of the Frank-Kamenetskii parameter increases with the Rayleigh number and heat transfer can be prevented by vigorous convection. In [8, 9], the influence of natural convection on the thermal instability of propagating reaction fronts was studied. These investigations focus on the determination of critical values of Rayleigh number and Lewis number demarcating a region of stability from that of instability. These were continued in [10, 11, 12] where new stationary and oscillating regimes were found. The authors showed how complex the regimes appeared through successive bifurcations leading from a stable stationary temperature distribution without convection to a stationary symmetric convective solution, stationary asymmetric convection, periodic in time oscillations, and finally aperiodic oscillations. Oscillating heat transfer, where the temperature grows and oscillates, was also discovered in the studies reported in [10, 11, 12]. The effects of natural convection and consumption of reactants on heat transfer in a closed spherical vessel were studied in [13]. Heat transfer with convection in a horizontal cylinder was considered in [14]. It should be stressed that, in these reference, the heat transfer is considered in a gaseous or liquid medium with its motion described by the Navier-Stokes equations under the Boussinesq approximation. In this study, the Darcy law in a quasi-stationary form under the Boussinesq approximation is used to describe fluid motion. It is shown that convection decreases the maximal temperature and increases the critical value of the Frank-Kamenetskii parameter.

In the current study, we consider a coupled Darcy and convection-diffusion system to model moving fronts in porous media. The system includes a wide variety of difficulties which typically arise in the numerical approximation of partial differential equations describing and consequently determining their dynamics. Current trends in incompressible viscous flows are to combine these equations with complex components to simulate applications, for instance, in fluid mechanics, groundwater, turbulence and multiphase flow models. All these applications require a very efficient and robust numerical solver for the convection-diffusion systems. Computing the numerical solution of the coupled system is not easy due to the nonlinear form, incompressibility condition and the presence of the convective terms. Hence, in many heat transfer equations, the convective term is distinctly more important than the diffusive term; particularly when the Peclet numbers reach high values, this convective term is a source of computational difficulties and oscillations. It is well known that the solutions of these equations present steep fronts which need to be resolved accurately in applications and often cause severe numerical difficulties. Modified method of characteristics or semi-Lagrangian methods as known in meteorological community, make use of the transport nature of the governing equations. They combine the fixed Eulerian grids with a particle tracking along the characteristic curves of the governing equations, see for instance [15, 16, 17, 18, 19]. The central idea in these methods is to rewrite the governing equations in terms of Lagrangian coordinates as defined by the particle trajectories (or characteristics) associated with the problem under consideration. The time derivative and the advection terms are combined as a directional derivative along the characteristics, leading to a characteristic time-stepping procedure. The Lagrangian treatment in these methods greatly reduces the time truncation errors in the Eulerian methods. Furthermore, the semi-Lagrangian method offers the possibility of using time steps that exceed those permitted by the Courant-Friedrichs-Lewy (CFL) stability condition in Eulerian methods for convection-dominated flows. A class of Galerkin-characteristic methods has been investigated in references [16, 20], among others. To this end, we examine the performance of Galerkin-characteristic finite element methods for numerical simulations of moving fronts in porous media under non-isothermal flow conditions. Unlike mixed finite elements, for which the different approximation spaces are used for the velocity field and the pressure variable, we present a unified finite element approximation for both solutions. This class of unified finite elements has been analyzed in [21, 22, 23] for Darcy and Stokes problems using a polynomial pressure-projection stabilization. The method consists of using the same low-order Eulerian finite element spaces to approximate both velocity and pressure solutions. In the current study, we extend and analyze these techniques in the framework of Galerkin-characteristic finite elements. For the temperature and concentration solutions we consider the L^2-projection in the host element where the departure points are located. Therefore, a second-order accuracy is achieved in the proposed Galerkin-characteristic unified finite element method for all the solution fields. Numerical results are presented for a class of Darcy flows problem with known analytical solutions to quantify the accuracy of the method. Then, the proposed Galerkin-characteristic unified finite element method is used to solve a coupled problem of moving thermal fronts in porous media. In the study, we also present analysis of convergence and stability for the proposed method and we give error estimates in the framework of L^2-theory.

The present paper is organized as follows. The description of the mathematical model is introduced in section 2. Section 3 is devoted to notations and preliminaries along with functional spaces and assumptions used in this study. This section includes also the finite element discretization of the spatial domain. In section 4 we formulate of the unified Galerkin-characteristic finite element method employed for the numerical solution of the Darcy problem and the convection-diffusion equations. Analysis of convergence and stability is presented in section 5. An optimal a priori error estimates in the L^2-norm is also investigated in this section. In section 6, we present numerical results for both two test problems with known exact solutions and the benchmark problem of moving fronts in porous media. Our new approach is shown to enjoy the expected accuracy as well as the robustness. Concluding remarks and perspectives are given in section 7.

2. Governing equations

A schematic of the physical system considered in the present work is shown in Figure 2.1. The system consists of a vertical rectangle enclosure with sides of height H, length L and subject to a thermal variation $(\Theta'_H - \Theta'_C)$, where Θ'_H and Θ'_C are temperatures of the hot and cold boundary walls. The enclosure consists of a Darcian fluid and all the thermo-physical properties are assumed to be constant, except for density in the buoyancy term that can be adequately modeled by the Boussinesq approximation. With these assumptions, the governing equations are:

Darcy equations:

$$\begin{aligned} u' &= -\frac{K_p}{\epsilon\mu}\frac{\partial p'}{\partial x'}, \\ v' &= -\frac{K_p}{\epsilon\mu}\left(\frac{\partial p'}{\partial y'} - \frac{g}{g_c}\beta\rho_0\left(\Theta' - \Theta'_0\right)\right), \\ \frac{\partial u'}{\partial x'} + \frac{\partial v'}{\partial y'} &= 0. \end{aligned} \tag{2.1}$$

Energy equation:

$$\rho_0 c_p\left(\epsilon\frac{\partial\Theta'}{\partial t'} + u'\frac{\partial\Theta'}{\partial x'} + v'\frac{\partial\Theta'}{\partial y'}\right) = \epsilon\lambda\left(\frac{\partial^2\Theta'}{\partial x'^2} + \frac{\partial^2\Theta'}{\partial y'^2}\right) + K(\Theta',\alpha')Q', \tag{2.2}$$

Depth of conversion equation:

$$\epsilon\frac{\partial\alpha'}{\partial t'} + u'\frac{\partial\alpha'}{\partial x'} + v'\frac{\partial\alpha'}{\partial y'} = \epsilon\gamma\left(\frac{\partial^2\alpha'}{\partial x'^2} + \frac{\partial^2\alpha'}{\partial y'^2}\right) + K(\Theta',\alpha'), \tag{2.3}$$

On the boundary, we consider the following conditions

$$\begin{aligned} &\Theta' = \Theta'_0, \quad \alpha' = 0 \quad \text{and} \quad \mathbf{u}' = 0 \quad \text{when} \quad y' \longrightarrow +\infty, \\ &\Theta' = \Theta'_\infty, \quad \alpha' = 1 \quad \text{and} \quad \mathbf{u}' = 0 \quad \text{when} \quad y' \longrightarrow -\infty. \end{aligned} \tag{2.4}$$

Here, the primed functions and variables refer to dimensional quantities. In the above equations, $\mathbf{u}' = (u', v')^\top$ is the velocity field, p' the pressure, Θ' is the temperature, α' the depth of conversion, K_p the permeability, ϵ the porosity, μ the dynamic viscosity, g the gravity force, β the coefficient of thermal expansion, ρ_0 the density, g_c a conversion constant, c_p the specific heat at constant pressure, λ the thermal conductivity coefficient, γ the depth diffusivity coefficient, Q' the adiabatic heat release, Θ'_0 the mean temperature and Θ'_∞ the reference temperature. In (2.2)-(2.3), the function $K(\Theta',\alpha') = \mathcal{K}(\Theta')\Phi(\alpha')$ describes the reaction rate where the temperature dependence is given by the Arrhenius law

$$\mathcal{K}(\Theta') = \epsilon k_0 \exp\left(-\frac{E}{R_0\Theta'}\right), \tag{2.5}$$

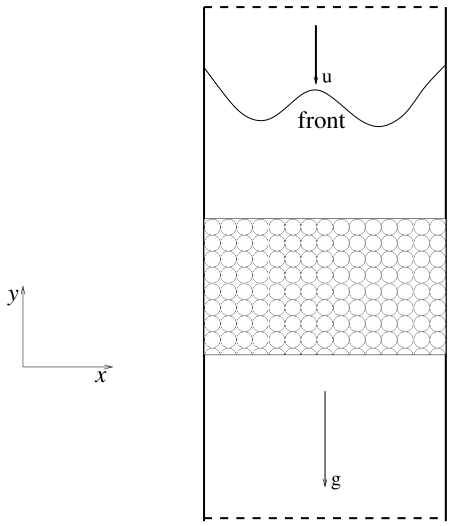

Figure 2.1: Illustration of the geometry for a moving front in porous media.

where k_0 is the pre-exponential factor, R_0 the universal gas constant and E is the activation energy assumed to be very large in the present study. The kinetic function $\Phi_\alpha(\alpha')$ is assumed to be independent of the reactant concentration and defined by the first-order reaction approximation as

$$\Phi_\alpha(\alpha') = 1 - \alpha', \quad 0 \leq \alpha' \leq 1. \tag{2.6}$$

Since it is convenient to work with dimensionless formulations, we define the following non-dimensional variables

$$x = \frac{x'c}{\kappa}, \quad y = \frac{y'c}{\kappa}, \quad t = \frac{t'c^2}{\kappa}, \quad \mathbf{u} = \frac{\mathbf{u}'}{\epsilon c}, \quad p = \frac{K_p p'}{\epsilon^2 \kappa \mu}, \quad \alpha = \alpha', \quad \Theta = \frac{\Theta' - \Theta'_\infty}{Q},$$

where the heat release Q and thermal diffusivity κ are defined as

$$Q = \frac{Q'}{\epsilon \rho_0 c_p} = \Theta'_H - \Theta'_C, \qquad \kappa = \frac{\lambda}{\rho_\infty c_p},$$

and c is the characteristic velocity given by [24]

$$c^2 = \frac{k_0 \kappa R_0 \Theta'^2_\infty}{QE} \exp\left(-\frac{E}{R_0 \Theta'^2_\infty}\right).$$

We also define the following dimensionless parameters

$$P_r = \frac{\mu}{\kappa}, \qquad R_a = \frac{\beta g Q \kappa^2}{\mu c^3}, \qquad R_p = \frac{K_p c^2 P_r R_a \rho_0}{\epsilon^2 \mu^2 g_c}, \qquad Z = \frac{QE}{R_0 \Theta'^2_\infty}, \qquad L_e = \frac{\kappa}{\gamma}, \quad \Theta_0 = \frac{\Theta'_\infty - \Theta'_0}{Q}, \quad \delta = \frac{R_0 \Theta'_\infty}{E},$$

where P_r, R_a, L_e and Z are the Prandtl number, the Rayleigh number, the Lewis number and the Zeldovich number, respectively. Hence, equations (2.1)-(2.4) can be rewritten in a coupled dimensionless form as

$$\begin{aligned} \mathbf{u} + \nabla p &= \mathbf{f}(\Theta), \\ \nabla \cdot \mathbf{u} &= 0, \end{aligned} \tag{2.7a}$$

$$
\begin{aligned}
\frac{D\Theta}{Dt} - \nabla^2\Theta &= g(\Theta, \alpha), \\
\frac{D\alpha}{Dt} - \frac{1}{L_e}\nabla^2\alpha &= g(\Theta, \alpha),
\end{aligned}
\tag{2.7b}
$$

where $\nabla = \left(\frac{\partial}{\partial x}, \frac{\partial}{\partial y}\right)^\top$ denotes the gradient operator and $\frac{D}{Dt}$ is the material derivative of any physical variable w defined by

$$
\frac{Dw}{Dt} = \frac{\partial w}{\partial t} + \mathbf{u} \cdot \nabla w. \tag{2.8}
$$

In the above and in what follows bold face type denotes vector quantities. Equations (2.7b)-(2.7a) are subject to the following boundary conditions

$$
\begin{aligned}
\Theta = -1, \quad \alpha = 0 \quad \text{and} \quad \mathbf{u} = 0 \quad \text{when} \quad y \longrightarrow +\infty, \\
\Theta = 0, \quad \alpha = 1 \quad \text{and} \quad \mathbf{u} = 0 \quad \text{when} \quad y \longrightarrow -\infty,
\end{aligned}
\tag{2.9}
$$

The function $\mathbf{f}$ in (2.7a) is defined by

$$
\mathbf{f}(\Theta) = R_p\,(\Theta + \Theta_0)\,\mathbf{e}, \tag{2.10}
$$

where $\mathbf{e}$ is the unit vector associated with the gravity and Θ_0 being a parameter with a constant value. In (2.7b), the function g is given by

$$
g(\Theta, \alpha) = W_Z\,(\Theta)\,\Phi_\alpha(\alpha), \tag{2.11}
$$

where $\Phi_\alpha(\alpha) = 1 - \alpha$, and the dimensionless reaction function $W_Z\,(\Theta)$

$$
W_Z\,(\Theta) = Z \exp\left(\frac{\Theta}{Z^{-1} + \delta\Theta}\right). \tag{2.12}
$$

It should be stressed that the exponent $-E/R_0\Theta'$ in the Arrhenius formula (2.5) represents the ratio between the activation energy E and the average kinetic energy $R_0\Theta'$. For most practical kinetic applications with highly exothermic reactions, the dependence on the temperature is negligible compared to the activation energy *i.e.*, $E >> R_0\Theta'$, see for example [24, 25]. Therefore, it becomes apparent with the negative sign in (2.5) that low rate is obtained for high values of this ratio. This ensures that a high activation energy yields less substantial effects on the exponential term and therefore its variation with temperature becomes very small. Thus, the dimensionless Arrhenius function (2.12) can be interpreted as a form of the exponential decay law. As a consequence, $g(\Theta, \alpha)$ in (2.11) is a bounded continuous real function which can be approximated by Lipschitz functions.

3. Preliminaries and assumptions

In this section, we introduce notations and assumptions to be used in this study. Let Ω be a bounded spatial domain in $\mathbb{R}^d$ ($d = 2, 3$) with Lipschitz boundary Γ, and $[0, T]$ is the time interval. For the time discretization we divide the time interval into N_T subintervals $[t_n, t_{n+1}]$ with length $\Delta t = t_{n+1} - t_n$ for $n = 0, 1, N_T$. We use the notation w^n to denote the value of a generic function w at time t_n. For solving the coupled equations (2.7), we first require a discretization of the space domain $\overline{\Omega} = \Omega \cup \Gamma$. Given h_0, $0 < h_0 < 1$, let h be a space discretization parameter such that $0 < h < h_0$. We generate a quasi-uniform partition, $\Omega_h \subset \bar{\Omega} = \Omega \cup \Gamma$, of finite elements $\mathcal{K}_j$ that satisfy the following conditions:

(i) $\overline{\Omega} = \bigcup_{j=1}^{Ne} \mathcal{K}_j$, where Ne is the number of elements of the partition Ω_h.

(ii) If $\mathcal{K}_i$ and $\mathcal{K}_j$ are two different elements of the partition Ω_h, then

$$
\mathcal{K}_i \cap \mathcal{K}_j = \begin{cases} P_{ij}, & \text{a mesh point, or} \\ \Gamma_{ij}, & \text{a common side, or} \\ \emptyset, & \text{empty set.} \end{cases}
$$

(iii) There exists a positive constant κ such that for all $j \in \{1, \cdots, Ne\}$, $\dfrac{d_j}{h_j} > \kappa$ $(h_j \le h)$, where d_j is the diameter of the circle inscribed in $\mathcal{K}_j$ and h_j is the largest side of $\mathcal{K}_j$.

The conforming finite element space for temperature, concentration and pressure is defined as

$$V_h = \Big\{ v_h \in C^0(\Omega) : \quad v_h\big|_{\mathcal{K}_j} \in P_k(\mathcal{K}_j), \quad \forall\, \mathcal{K}_j \in \Omega_h \Big\},$$

where $P_k(\mathcal{K}_j)$ is the space of complete polynomials of degree k defined in $\mathcal{K}_j$. We also define the conforming finite element space $\mathbf{V}_h$ for the velocity field as

$$\mathbf{V}_h = V_h \times V_h.$$

We use the notation w^n to denote the value of a generic function w at time t_n. Hence, we formulate the finite element solutions to $\mathbf{u}^n(\mathbf{x})$, $\Theta^n(\mathbf{x})$, $\alpha^n_h(\mathbf{x})$ and $p^n(\mathbf{x})$ as

$$\mathbf{u}^n_h(\mathbf{x}) = \sum_{j=1}^{M} U^n_j \cdot \varphi_j(\mathbf{x}), \quad \Theta^n_h(\mathbf{x}) = \sum_{j=1}^{M} \mathcal{T}^n_j \phi_j(\mathbf{x}), \quad \alpha^n_h(\mathbf{x}) = \sum_{j=1}^{M} \mathcal{A}^n_j \phi_j(\mathbf{x}), \quad p^n_h(\mathbf{x}) = \sum_{j=1}^{M} P^n_j \phi_j(\mathbf{x}), \tag{3.1}$$

The functions U^n_j, $\mathcal{T}^n_j$, $\mathcal{A}^n_j$ and P^n_j are the corresponding nodal values of $\mathbf{u}^n_h(\mathbf{x})$, $\Theta^n_h(\mathbf{x})$, $\alpha^n_h(\mathbf{x})$ and $p^n_h(\mathbf{x})$, respectively. They are defined as $U^n_j = \mathbf{u}^n_h(\mathbf{x}_j)$, $\mathcal{T}^n_j = \Theta^n_h(\mathbf{x}_j)$, $\mathcal{A}^n_j = \alpha^n_h(\mathbf{x}_j)$ and $P^n_j = p^n_h(\mathbf{x}_j)$ where $\{\mathbf{x}_j\}_{j=1}^M$ is the set of mesh points in the partition Ω_h. In (3.1), $\{\varphi_j\}_{j=1}^M = \{(\phi_j, \phi_j)\}_{j=1}^M$ and $\{\phi_j\}_{j=1}^M$ are the basis vectors and functions of $\mathbf{V}_h$ and V_h respectively given by the Kronecker delta symbol.

We shall use standard notation for Sobolev spaces, norms, and inner products. Here, C, C', C'', $C1, \ldots$ are used to denote generic positive constants independent of the mesh parameter h whose values may change from place to place. We also use the notation $|\cdot|$ to denote the standard Euclidean norm in $\mathbb{R}^d$. The functional spaces $C^k(\Omega)$, $k \ge 1$ refer to the class of functions whose partial derivatives of order at least k are bounded and uniformly continuous in Ω, whereas $C^k_0(\Omega)$ denotes the set of compactly supported functions contained in $C^k(\Omega)$. We also define the Sobolev spaces $W^{m,p}(\Omega)$ for any integers (m, p), $m \ge 1$ and $1 \le p \le \infty$ as

$$W^{m,p}(\Omega) = \Big\{ \mathbf{w} \in L^p(\Omega)^d : \qquad D^k\mathbf{w} \in L^p(\Omega)^d, \quad \forall\ |k| \le m \Big\},$$

where $k = (k_1, \ldots, k_d) \in \mathbb{N}^d$ is a multi-index of order $|k| = k_1 + \cdots + k_d$, and the derivative operator D^k is given by

$$D^k = \frac{\partial^{|k|}}{\partial x_1^{k_1} \cdots \partial x_d^{k_d}}.$$

These spaces are equipped with the following norms

$$\|\mathbf{w}\|_{m,p} = \begin{cases} \left(\displaystyle\sum_{0 \le |k| \le m} \left\| D^k\mathbf{w} \right\|^p_{L^p(\Omega)} \right)^{\frac{1}{p}}, & \text{if} \quad 1 \le p < \infty, \\[2ex] \displaystyle\max_{\mathbf{x} \in \Omega, 0 \le |k| \le m} \left\| D^k\mathbf{w} \right\|_{L^\infty(\Omega)}, & \text{if} \quad p = \infty, \end{cases}$$

and the semi-norms

$$|\mathbf{w}|_{m,p} = \begin{cases} \left(\displaystyle\sum_{|k| = m} \left\| D^k\mathbf{w} \right\|^p_{L^p(\Omega)} \right)^{\frac{1}{p}}, & \text{if} \quad 1 \le p < \infty, \\[2ex] \displaystyle\max_{\mathbf{x} \in \Omega, |k| = m} \left\| D^k\mathbf{w} \right\|_{L^\infty(\Omega)}, & \text{if} \quad p = \infty. \end{cases}$$

Note that, in the special case $p = 2$, the space $W^{m,2}(\Omega)$ $(m \geq 1)$ forms the Hilbert space $H^m(\Omega)$ which is the closure of $C^\infty(\Omega)$. We also define $H_0^m(\Omega)$ as the closure of $C_0^\infty(\Omega)$ with respect to the same norm. For $m = 1$, $H^{-1}(\Omega)$ denote the dual space of $H_0^1(\Omega)$ and the space $L^2(\Omega)$ is defined by

$$L^2(\Omega) = \left\{ w : \ \Omega \longrightarrow \mathbb{R} : \qquad \int_\Omega w^2 d\Omega < \infty \right\},$$

whose inner product and norm are defined by

$$(w, v) = \int_\Omega wv \, d\Omega \qquad \text{and} \qquad \|w\|_{L^2(\Omega)} = (w, w)^{\frac{1}{2}}, \qquad \forall \ w, v \in L^2(\Omega),$$

respectively. We also define the space $L_0^2(\Omega)$ of all square integrable functions with vanishing mean as

$$L_0^2(\Omega) = \left\{ w : \ \Omega \longrightarrow \mathbb{R} : \qquad \int_\Omega w d\Omega = 0 \right\}.$$

For the Darcy problem, we recall the standard spaces $\mathbf{H}(div, \Omega)$ and $\mathbf{H}_0(div, \Omega)$

$$\mathbf{H}(div, \Omega) = \left\{ \mathbf{w} \in (L^2(\Omega))^d : \qquad div(\mathbf{w}) \in L^2(\Omega) \right\}, \qquad \mathbf{H}_0(div, \Omega) = \left\{ \mathbf{w} \in \mathbf{H}(div, \Omega) : \qquad (\mathbf{w} \cdot \mathbf{n})\Big|_\Gamma = 0 \right\}.$$

For the convection-diffusion equations, we introduce the following spaces

$$H^1(\Omega) = \left\{ w \in L^2(\Omega) : \qquad \partial^k w \in L^2(\Omega), \quad \forall \ |k| \leq 1 \right\}, \qquad H_0^1(\Omega) = \left\{ w \in H^1(\Omega) : \qquad \mathbf{w}|_\Gamma = 0 \right\}.$$

For a real Banach space X and $1 \leq p \leq \infty$ we introduce the standard Bochner spaces $L^p(0, T; X)$ consisting of all measurable functions $w(t, \mathbf{x})$ defined in $[0, T] \times \Omega$ for which

$$\begin{aligned} \int_0^T \|w\|_X^p dt &< \infty, \qquad \text{if} \quad 1 \leq p < \infty, \\ \operatorname*{ess\ sup}_{t \in [0,T]} \|w(\cdot, t)\|_X &< \infty, \qquad \text{if} \quad p = \infty. \end{aligned}$$

Here, the space $L^p(0, T; X)$ is equipped with the norm

$$\|w\|_{L^p(0,T;X)} = \begin{cases} \left(\displaystyle\int_0^T \|w\|_X^p dt \right)^{1/p}, & \text{if} \quad 1 \leq p < \infty, \\ \operatorname*{ess\ sup}_{t \in [0,T]} \|w(\cdot, t)\|, & \text{if} \quad p = \infty. \end{cases}$$

It should be noted that the previous notations concern scalar functions and can be extended to d-dimensional vector functions in a similar way by using the product norms. In what follows, we announce the assumptions required for the analysis in the present study.

Assumption **3.1.** *The temperature Θ and the concentration α are assumed to satisfy:*

1. $\Theta \in L^\infty \left(0, T; H^{m+1} \cap W^{m+1,\infty}(\Omega)\right)$ *and* $\alpha \in L^\infty \left(0, T; H^{m+1} \cap W^{m+1,\infty}(\Omega)\right)$,
2. $\dfrac{D^2\Theta}{Dt^2} \in L^2 \left(0, T; L^2(\Omega)\right)$ *and* $\dfrac{D^2\alpha}{Dt^2} \in L^2 \left(0, T; L^2(\Omega)\right)$,
3. $\dfrac{D^3\Theta}{Dt^3} \in L^2 \left(0, T; L^2(\Omega)\right)$ *and* $\dfrac{D^3\alpha}{Dt^3} \in L^2 \left(0, T; L^2(\Omega)\right)$.

Assumption **3.2.** *The velocity field* $\mathbf{u}$ *is assumed to satisfy:*

1. $\mathbf{u}(\mathbf{x},t) \in C^0\left(0,T;W^{1,\infty}(\Omega)\right)$,
2. $\nabla \cdot \mathbf{u}(\mathbf{x},t) = 0$ *in* Ω,
3. $\mathbf{u}(\mathbf{x},t)\cdot \mathbf{n} = 0$ *on* $\partial\Omega$.

Assumption **3.3.** *The functions* $\mathbf{f}$ *and* g *defined in* (2.10) *and* (2.11) *are assumed to verify:*

1. $\mathbf{f} \in L^2\left(0,T;L^2(\Omega)^d\right)$ *and* $g \in L^2\left(0,T;L^2(\Omega)\right)$
2. $\mathbf{f}$ *is Lipschitz with respect to its variable* Θ *i.e.,*

$$\|\mathbf{f}(\Theta)\|_{L^\infty(0,T;L^2(\Omega)^d)} \leq c_{\mathbf{f}}\ \|\Theta\|_{L^\infty(0,T;L^2(\Omega)^d)}\,,$$

where $c_{\mathbf{f}}$ *is a positive constant.*

3. g *is Lipschitz with respect to its variables* (Θ,α) *i.e.,*

$$\|g(\Theta,\alpha)\|_{L^\infty(0,T;L^2(\Omega))} \leq c_g \left(\ \|\Theta\|_{L^\infty(0,T;L^2(\Omega))} + \|\alpha\|_{L^\infty(0,T;L^2(\Omega))}\right),$$

where c_g *is a positive constant.*

Finally, we introduce the operators required for the error analysis of the temperature and concentration solutions. Hence, assuming that the subset V_h is composed of polynomials of degree $k \geq 2$ on each element $\mathcal{K}_j$, $j=1,\cdots N_e$ of the partition Ω_h. For $w=\Theta$ or α, we define the following operators:

- The orthogonal projection operator $P_0 : H^{-1}(\Omega) \longrightarrow V_h$

$$(P_0 w,\phi) = (w,\phi)\,, \qquad \forall\ \phi \in V_h. \tag{3.2}$$

- The polynomial interpolant of degree m for continuous functions $w \in V_h$, $I_m :\ C^0(\overline{\Omega}) \longrightarrow V_h$

$$I_m w(\mathbf{x}) = \sum_{j=1}^{M} w(\mathbf{x}_j)\phi_j(\mathbf{x}), \qquad \forall\ \mathbf{x} \in \overline{\Omega}, \tag{3.3}$$

  where $\mathbf{x}_j$ $(1 \leq j \leq M)$ are mesh points in the partition Ω_h. Then, by the approximation theory, we have

$$\|w - I_m w\|_{L^2(\Omega)} \leq Ch^{m+1}|w|_{m+1}. \tag{3.4}$$

- The linear continuous operator $A :\ H_0^1(\Omega) \longrightarrow H^{-1}(\Omega)$

$$\langle Aw, r\rangle = (\nabla w, \nabla r)\,, \qquad \forall\ r \in H_0^1(\Omega), \tag{3.5}$$

  where $\langle\cdot,\cdot\rangle$ denotes the duality pairing. It is evident that A is a symmetric positive definite operator on $H_0^1(\Omega)$.

- The discrete operator $A_h :\ V_h \longrightarrow V_h$,

$$(A_h w_h, \phi) = \langle A w_h, \phi\rangle\,, \qquad \forall\ \phi \in V_h. \tag{3.6}$$

  A_h is also a symmetric positive definite operator on V_h.

- The Ritz projection operator $R :\ V_h \longrightarrow V_h$,

$$(\nabla w, \nabla r) = \langle A w_h, \phi\rangle\,, \qquad \forall\ \phi \in V_h. \tag{3.7}$$

- The discrete operator $G_h : V_h \longrightarrow V_h$,

$$(g_h(w),\phi) = (g(w),\phi), \qquad \forall\ \phi \in V_h. \tag{3.8}$$

Note that it is easy to verify that

$$A_h R = P_0 A \qquad \text{and} \qquad G_h = P_0 g.$$

It should also be stressed that the assumptions introduced above are needed in the current work in order to analyze convergence and stability of the proposed Galerkin-characteristic unified finite element method for the coupled Darcy and convection-diffusion-reaction problems (2.7). These assumptions are also used to establish error estimates for velocity, pressure, temperature and concentration solutions.

4. Galerkin-characteristic unified finite element method

As in most finite element methods, the starting point in the Galerkin-characteristic unified finite element method is the weak formulation of the problem under study. Hence, the weak formulation of the coupled problem (2.7) reads: Find the quadruplet $(\mathbf{u}, p, \Theta, \alpha)$ in $\mathbf{H}_0(div, \Omega) \times L_0^2(\Omega) \times H_0^1(\Omega) \times H_0^1(\Omega)$ such that

$$
\begin{aligned}
\int_\Omega \mathbf{u}\cdot\mathbf{s}\, d\Omega - \int_\Omega p\nabla\cdot\mathbf{s}\, d\Omega &= \int_\Omega \mathbf{f}(\Theta)\cdot\mathbf{s}\, d\Omega, && \forall\, \mathbf{s}\in\mathbf{H}_0(div,\Omega),\\
\int_\Omega q\,\nabla\cdot\mathbf{u}\, d\Omega &= 0, && \forall\, q\in L_0^2(\Omega),
\end{aligned}
\tag{4.1a}
$$

$$
\begin{aligned}
\int_\Omega \frac{D\Theta}{Dt} r\, d\Omega + \int_\Omega \nabla\Theta\cdot\nabla r\, d\Omega &= \int_\Omega g(\Theta,\alpha) r\, d\Omega, && \forall\, r\in H_0^1(\Omega),\\
\int_\Omega \frac{D\alpha}{Dt} r\, d\Omega + \frac{1}{L_e}\int_\Omega \nabla\alpha\cdot\nabla r\, d\Omega &= \int_\Omega g(\Theta,\alpha) r\, d\Omega, && \forall\, r\in H_0^1(\Omega).
\end{aligned}
\tag{4.1b}
$$

It evident that any quadruplet $(\mathbf{u}, p, \Theta, \alpha) \in \mathbf{H}_0(div, \Omega) \times L_0^2(\Omega) \times H_0^1(\Omega) \times H_0^1(\Omega)$ solving the problem (2.7) in the sense of distributions in Ω is a solution of the variational problem (4.1). For the a priori bound on the temperature Θ and concentration α we have the following theorem:

Theorem **4.1.** *Every solution of* (4.1) *such that* $(\Theta, \alpha) \in L^\infty(\Omega\times[0,T]) \times L^\infty(\Omega\times[0,T])$ *satisfies the following bounds:*

$$
\|\mathbf{u}\|_{L^2(\Omega)^d} \le c_{\mathbf{f}}\, \|\Theta\|_{L^\infty(0,T;L^2(\Omega)^d}\,, \tag{4.2}
$$

$$
\|\Theta\|^2_{L^\infty(0,T;L^2(\Omega))} + \|\Theta\|^2_{L^2(0,T;H_0^1(\Omega))} \le c_g\left(\frac{3}{2}\|\Theta\|^2_{L^2(0,T;L^2(\Omega))} + \frac{1}{2}\|\alpha\|^2_{L^2(0,T;L^2(\Omega))}\right), \tag{4.3}
$$

and

$$
\|\alpha\|^2_{L^\infty(0,T;L^2(\Omega))} + \frac{1}{L_e}\|\alpha\|^2_{L^2(0,T;H_0^1(\Omega))} \le c_g\left(\frac{3}{2}\|\alpha\|^2_{L^2(0,T;L^2(\Omega))} + \frac{1}{2}\|\Theta\|^2_{L^2(0,T;L^2(\Omega))}\right), \tag{4.4}
$$

where $c_{\mathbf{f}}$ and c_g are positive constants independent of h. □

Proof. By testing equations (4.1a) with $\mathbf{s} = \mathbf{u}$ and $q = p$, and using the Cauchy-Schwarz inequality together with Assumption 3.3 on the function $\mathbf{f}$ we immediately derive the a priori bound (4.2). Next, for $\mathbf{u} \in \mathbf{H}_0(div, \Omega)$ rewriting the first equation in (4.1b) by using the definition of the material derivative (2.8) and testing it with $r = \Theta$, we obtain by noting that $\int_\Omega(\mathbf{u}\cdot\nabla\Theta)\Theta\, d\Omega = 0$ and using the Cauchy-Schwarz inequality for all $t \in [0, T]$

$$
\frac{1}{2}\frac{d}{dt}\|\Theta\|^2_{L^2(\Omega)} + \|\nabla\Theta\|^2_{L^2(\Omega)} \le \|g(\Theta,\alpha)\|_{L^2(\Omega)}\, \|\Theta\|_{L^2(\Omega)}\,.
$$

Then, by using Assumption 3.3 on the function g along with the well-known Young's inequality $\left(ab \le \frac{a^2}{2} + \frac{b^2}{2}\right)$, we easily obtain (4.3). Note that (4.4) can be derived in the same manner by testing the second equation in (4.1b) with $r = \alpha$.
■

In the present study, to approximate solutions of the coupled problem (4.1) in space, we use the unified Galerkin-characteristic finite element method which consists of using the same polynomial approximation for temperature, concentration, velocity and pressure solutions in the simplicial finite elements $\mathcal{K}_j$ in Ω_h. The conforming finite element spaces that we use are polynomials P_k of the same degree k for all the solutions defined on the element $\mathcal{K}_j$. Thus, to approximate the velocity and pressure solutions for the Darcy problem (4.1a), we consider the equal-order pair $(\mathbf{S}_h, Q_h)$ with

$$
\mathbf{S}_h = \mathbf{V}_h \cap \mathbf{H}_0\,(div,\Omega) \qquad \text{and} \qquad Q_h = V_h \cap L_0^2(\Omega). \tag{4.5}
$$

To approximate the temperature and concentration solutions for the convection-diffusion-reaction problem (4.1b), we define the discrete space R_h as

$$R_h = V_h \cap H_0^1(\Omega). \tag{4.6}$$

Note that same finite elements are used for solving both the Darcy problem and the convection-diffusion-reaction equations without requiring mixed formulations widely used in the literature, see for example [26, 27]. This results in a simple and efficient implementation of the method without need for mixed finite element techniques.

4.1. Solution of the Darcy problem

The Darcy problem (4.1a) can be reformulated as

$$\begin{aligned} \mathcal{A}(\mathbf{u}_h, \mathbf{s}_h) - \mathcal{B}(p_h, \mathbf{s}_h) &= \mathcal{L}_{\mathbf{f}}(\mathbf{s}_h), & \forall\, \mathbf{s}_h \in \mathbf{S}_h, \\ \mathcal{B}(q_h, \mathbf{u}_h) &= 0, & \forall\, q_h \in Q_h, \end{aligned} \tag{4.7}$$

where $\mathcal{A}$, $\mathcal{B}$ are the bilinear forms and $\mathcal{L}_{\mathbf{f}}$ is the linear form defined as

$$\mathcal{A}(\mathbf{u}_h, \mathbf{s}_h) = \int_\Omega \mathbf{u}_h \cdot \mathbf{s}_h \, d\Omega, \quad \mathcal{B}(p_h, \mathbf{s}_h) = \int_\Omega p_h \nabla \cdot \mathbf{s}_h \, d\Omega, \quad \mathcal{L}_{\mathbf{f}}(\mathbf{s}_h) = \int_\Omega \mathbf{f}_h \cdot \mathbf{s}_h \, d\Omega.$$

Note that a stable and accurate solution of the discrete problem (4.7) requires that the spaces $\mathbf{S}_h$ and Q_h satisfy the discrete inf-sup condition [28],

$$\sup_{\substack{\mathbf{s}_h \in \mathbf{S}_h \\ \mathbf{s}_h \neq 0}} \frac{\mathcal{B}(p_h, \mathbf{s}_h)}{\|\mathbf{s}_h\|_{H^1(\Omega)^d}} \geq C \, \|p_h\|_{L^2(\Omega)}, \qquad \forall\, p_h \in Q_h, \tag{4.8}$$

with $C > 0$ being a constant independent of h. However, it is well known that the pair $(\mathbf{S}_h, Q_h)$ does not verify the inf-sup condition associated with the mixed form (4.7), see [29, 30, 21] for further details. Therefore, the discrete weak problem is not stable and a stabilization techniques is required. In the current work, to stabilize (4.7) we use the polynomial pressure-projection stabilization method introduced in [21, 22]. The method consists of defining a local L^2-projection operator onto the discontinuous polynomial space as

$$[P]_{k-1} = \left\{ q_h \in L^2(\Omega) : \quad q_h \Big|_{\mathcal{K}_j} \in P_{k-1}(\mathcal{K}_j), \quad \forall\, \mathcal{K}_j \in \Omega_h \right\},$$

where the projection operator $\Pi_{k-1} : \ L^2(\Omega) \longrightarrow [P]_{k-1}$ is defined by

$$\Pi_{k-1}(p) = \arg\min \frac{1}{2} \int_\Omega \left(\Pi_{k-1} q_h - p \right)^2 \, d\Omega. \tag{4.9}$$

Using this local projection, the velocity-pressure space $(\mathbf{S}_h, Q_h)$ verifies a stabilized form of the inf-sup condition (4.8). Thus, we recall the following result whose proofs can be found the proof in [21].

Lemma **4.1.** *Let $\mathbf{S}_h$ and Q_h be the spaces defined in* (4.5)*. Then, there exist positive constants C_1 and C_2 whose values are independent of h such that*

$$\sup_{\substack{\mathbf{s}_h \in \mathbf{S}_h \\ \mathbf{s}_h \neq 0}} \frac{\mathcal{B}(p_h, \mathbf{s}_h)}{\|\mathbf{s}_h\|_{H^1(\Omega)^d}} \geq C_1 \, \|p_h\|_{L^2(\Omega)} - C_2 \, \|p_h - \Pi_{k-1} p_h\|_{L^2(\Omega)}, \qquad \forall\, p_h \in Q_h. \quad \blacksquare \tag{4.10}$$

Note that the stabilized inf-sup condition (4.10) allows to identify terms that can be used to stabilize the unified finite element method considered in this study. Furthermore, other than the range assumption, Lemma 4.1 requires no additional hypotheses on the projection operator Π_{k-1}, compare [21]. Hence, the stabilized weak form reads: Find $(\mathbf{u}_h, p_h) \in \mathbf{S}_h \times Q_h$ such that

$$\begin{aligned} \mathcal{A}(\mathbf{u}_h, \mathbf{s}_h) - \mathcal{B}(p_h, \mathbf{s}_h) &= \mathcal{L}_{\mathbf{f}}(\mathbf{s}_h), \qquad \forall\ \mathbf{s}_h \in \mathbf{S}_h, \\ \mathcal{B}(q_h, \mathbf{u}_h) &= \mathcal{D}(p_h, q_h), \qquad \forall\ q_h \in Q_h, \end{aligned} \tag{4.11}$$

where $\mathcal{D}$ is the bilinear form defined as

$$\mathcal{D}(p_h, q_h) = \int_\Omega (p_h - \Pi_{k-1} p_h)(q_h - \Pi_{k-1} q_h)\ d\Omega.$$

It should be stressed that, this unified finite element method has been assessed and examined for several examples for stokes and Darcy problems and the obtained results have shown that the method is efficient, accurate and stable, see [21, 22, 23] among others.

4.2. Solution of the convection-diffusion problem

To solve the convection-diffusion equations (4.1b), we consider the Galerkin-characteristic method using the modified method of characteristics for the convection terms. This class of method have been used for solving many convection-dominated flow problems, see for example [15, 16, 20, 31, 32, 33]. Here, the main idea is to decouple the transport parts $\frac{D\Theta}{Dt}$ and $\frac{D\alpha}{Dt}$ from the convection-diffusion equations (4.1b) in the finite element discretization. The new temperature and concentration solutions are approximated at each time subinterval $[t_n, t_{n+1}]$ using the characteristic curves associated with the material derivative (2.8). Here, the characteristic curves $\mathcal{X}(\mathbf{x}, t_{n+1}; t)$ associated with the material derivative (2.8) are the solutions of the ordinary differential equations

$$\begin{aligned} \frac{d\mathcal{X}(\mathbf{x}, t_{n+1}; t)}{dt} &= \mathbf{u}(t, \mathcal{X}(\mathbf{x}, t_{n+1}; t)), \qquad \forall\ (t, \mathbf{x}) \in [t_n, t_{n+1}] \times \bar{\Omega}, \\ \mathcal{X}(\mathbf{x}, t_{n+1}; t_{n+1}) &= \mathbf{x}. \end{aligned} \tag{4.12}$$

The solutions are called departure points at time t of a particle passing through the point $\mathbf{x}$ at time $t = t_{n+1}$. Note that we assume that the velocity field $\mathbf{u}$ satisfies Assumption 3.2 which guarantees the existence and uniqueness of the solution of (4.12) for all times t, see for instance [34]. Then, the unique solution of (4.12) can be expressed for all $(t, \mathbf{x})$ in $[t_n, t_{n+1}] \times \bar{\Omega}$ as

$$\mathcal{X}(\mathbf{x}, t_{n+1}; t_n) = \mathbf{x} - \int_{t_n}^{t_{n+1}} \mathbf{u}(t, \mathcal{X}(\mathbf{x}, t_{n+1}; t))\, dt, \tag{4.13}$$

To obtain the departure points $\{\mathcal{X}^n_{hj}\}$ for each mesh point $\mathbf{x}_j$, $j = 1, \ldots, M$, we use the algorithm proposed in [19] which accurately solves (4.12) with a second-order accuracy. We write the solution of (4.12) in the form of

$$\mathcal{X}^n_{hj} = \mathbf{x}_j - \mathbf{d}_{hj}, \qquad j = 1, \ldots, M, \tag{4.14}$$

where the displacement $\mathbf{d}_{hj}$ is calculated by the iterative procedure

$$\begin{aligned} \mathbf{d}^{(0)}_{hj} &= \frac{\Delta t}{2}\Big(3\mathbf{u}^n_h\big(\mathbf{x}_j\big) - \mathbf{u}^{n-1}_h\big(\mathbf{x}_j\big)\Big), \\ \mathbf{d}^{(k+1)}_{hj} &= \frac{\Delta t}{2}\left(3\mathbf{u}^n_h\left(\mathbf{x}_j - \frac{1}{2}d^{(k)}_{hj}\right) - \mathbf{u}^{n-1}_h\left(\mathbf{x}_j - \frac{1}{2}d^{(k)}_{hj}\right)\right), \qquad k = 0, 1, \ldots. \end{aligned} \tag{4.15}$$

To evaluate values of the approximate velocities $\mathbf{u}^n_h\left(\mathbf{x}_j - \frac{1}{2}\mathbf{d}^{(k)}_{hj}\right)$ and $\mathbf{u}^{n-1}_h\left(\mathbf{x}_j - \frac{1}{2}\mathbf{d}^{(k)}_{hj}\right)$ in (4.15), we first identify the mesh element $\widehat{\mathcal{K}}_j$ where $\mathbf{x}_j - \frac{1}{2}\mathbf{d}^{(k)}_{hj}$ resides. Then, a finite element interpolation on $\widehat{\mathcal{K}}_j$ is carried out according to (3.1). In the numerical simulations obtained, the iterations in (4.15) were continued until the trajectory changed by less than 10^{-7}. However, in practice it is not recommended to repeat the iteration process more than a few times due to efficiency considerations.

We assume that the pairs $(\mathcal{X}^n_{hj}, \widehat{\mathcal{K}}_j)$ along with the mesh point values $\left\{\mathcal{T}^n_j, \mathcal{A}^n_j\right\}$ are known for all $j = 1, \ldots, M$, we compute the values $\left\{\widehat{\mathcal{T}}^n_j, \widehat{\mathcal{A}}^n_j\right\}$ as

$$\widehat{\mathcal{T}}^n_j := \Theta^n_h(\mathcal{X}^n_{hj}) = \sum_{k=1}^{M} \mathcal{T}_k \phi(\mathcal{X}^n_{hj}), \qquad \widehat{\mathcal{A}}^n_j := \alpha^n_h(\mathcal{X}^n_{hj}) = \sum_{k=1}^{M} \mathcal{A}_k \phi(\mathcal{X}^n_{hj}). \tag{4.16}$$

Then, the solution $\left\{\widehat{\Theta}^n_h(\mathbf{x}), \widehat{\alpha}^n_h(\mathbf{x})\right\}$ of the convection equations (2.7b) is obtained by

$$\widehat{\Theta}^n_h(\mathbf{x}) = \sum_{j=1}^{M} \widehat{\mathcal{T}}^n_j \phi_j(\mathbf{x}), \qquad \widehat{\alpha}^n_h(\mathbf{x}) = \sum_{j=1}^{M} \widehat{\mathcal{A}}^n_j \phi_j(\mathbf{x}). \tag{4.17}$$

In transient Darcian flow problems, the convection process is repeated continuously. Thus, some artifacts which can be tolerated for one step might become a serious issue as the errors start building up after several steps. Indeed, if the solution of Darcian flow equations is expected to have sharp gradients, the numerical solution obtained by the conventional Galerkin-characteristic method either develops spurious oscillations or it is affected by a large artificial viscosity. Spurious oscillations and artificial viscosity often deteriorate the accuracy of the solution, so the numerical solution may become physically unacceptable. For this reason, in most Galerkin-characteristic methods linear interpolation procedures result in an oscillation-free solutions. However, applied to the Darcian flow equations a Galerkin-characteristic method would require higher order interpolation for a higher accuracy. The main problem with the high-order interpolation procedures is that high degree polynomials they use might show oscillatory behavior as they are forced to satisfy the continuity condition at the nodal points. In order to avoid the principal drawback of the conventional Galerkin-characteristic methods (4.16), that is the failure to preserve monotonicity, we incorporate an L^2-projection into our algorithm to convert the method to non-oscillatory and shape preserving at an additional computational cost. The procedure consists of evaluating $\widehat{\Theta}^n_h$ and $\widehat{\alpha}^n_h$ in (4.17) using an L^2-projection on the space V_h. The method uses ideas of the quadrature rules for the approximation of integrals in the finite element discretization.

In the current study, the Galerkin-characteristic L^2-projection method consists of generating a virtual partition $\widehat{\Omega}^n_h = \mathcal{X}^n(\Omega_h)$ that is the image of the fixed mesh partition Ω_h composed of elements $\widehat{\mathcal{K}}^n_j = \mathcal{X}^n\left(\mathcal{K}_j\right)$, *i.e.*

$$\widehat{\Omega}^n_h = \left\{\widehat{\mathcal{K}}^n_j \subset \mathcal{X}^n\left(\bar{\Omega}\right): \qquad \widehat{\mathcal{K}}^n_j = \mathcal{X}^n\left(\mathcal{K}_j\right), \quad j = 1, \ldots, Ne\right\}.$$

Then, we define the finite element space $\widehat{V}^n_h$ associated with $\widehat{\Omega}^n_h$ as

$$\widehat{V}^n_h = \left\{\widehat{v}^n_h \in C^0\left(\mathcal{X}^n(\Omega_h)\right): \quad \widehat{v}^n_h\big|_{\widehat{\mathcal{K}}^n_j} \in S(\widehat{\mathcal{K}}^n_j), \quad \forall\, \widehat{\mathcal{K}}^n_j \in \widehat{\Omega}^n_h\right\}.$$

Given $(\Theta^n(\mathbf{x}), \alpha^n(\mathbf{x})) \in V_h \times V_h$ the approximate solutions of the problem at the current time t_n, and denoting by $\left(\widehat{P}^n_h\Theta^n(\mathcal{X}^n), \widehat{P}^n_h\alpha^n(\mathcal{X}^n)\right)$ the approximations of the L^2-projection of $(\Theta^n(\mathcal{X}^n), \alpha^n(\mathcal{X}^n))$ onto $\widehat{\Omega}^n_h \times \widehat{\Omega}^n_h$, then the solutions $\left(\Theta^{n+1}(\mathbf{x}), \alpha^{n+1}(\mathbf{x})\right) \in V_h \times V_h$ at time t_{n+1} are approximated by

$$\Theta^{n+1}(\mathbf{x}) = \widehat{\mathcal{P}}^n_h\Theta^n(\mathcal{X}^n), \qquad \alpha^{n+1}(\mathbf{x}) = \widehat{\mathcal{P}}^n_h\alpha^n(\mathcal{X}^n). \tag{4.18}$$

Thus, to any pair functions $\left(\widehat{\Theta}^n_h, \widehat{\alpha}^n_h\right) \in \widehat{V}^n_h \times \widehat{V}^n_h$, where

$$\widehat{\Theta}^n_h(\mathcal{X}) = \sum_{j=1}^{M} \widehat{\mathcal{T}}^n_j \widehat{\phi}_j(\mathcal{X}), \qquad \widehat{\alpha}^n_h(\mathcal{X}) = \sum_{j=1}^{M} \widehat{\mathcal{A}}^n_j \widehat{\phi}_j(\mathcal{X}),$$

there corresponds a pair functions $\left(\widetilde{\Theta}^{n+1}_h(\mathbf{x}), \widetilde{\alpha}^{n+1}_h(\mathbf{x})\right) \in V_h \times V_h$ defined by

$$\widetilde{\Theta}^{n+1}_h(\mathbf{x}) = \sum_{j=1}^{M} \widehat{\mathcal{T}}^n_j \phi_j(\mathbf{x}), \qquad \widetilde{\alpha}^{n+1}_h(\mathbf{x}) = \sum_{j=1}^{M} \widehat{\mathcal{A}}^n_j \phi_j(\mathbf{x}).$$

Next, we consider the solutions $\mathcal{T}^n(\mathcal{X}^n)$ and $\mathcal{A}^n(\mathcal{X}^n)$ which are continuous in Ω but do not belong to $\widehat{V}_h^n$. Define $\left(\widehat{\Theta}_h^n, \widehat{\alpha}_h^n\right) \in \widehat{V}_h^n \times \widehat{V}_h^n$ as the L^2-projection of $\left(\mathcal{T}^n(\mathcal{X}^n), \mathcal{A}^n(\mathcal{X}^n)\right)$ onto $\widehat{V}_h^n \times \widehat{V}_h^n$ such that, for all $\widehat{v}_h^n \in \widehat{V}_h^n$

$$\left\langle \widehat{\Theta}_h^n(\mathcal{X}), \widehat{v}_h^n(\mathcal{X}) \right\rangle = \left\langle \mathcal{T}^n(\mathcal{X}), \widehat{v}_h^n(\mathcal{X}) \right\rangle, \qquad \left\langle \widehat{\alpha}_h^n(\mathcal{X}), \widehat{v}_h^n(\mathcal{X}) \right\rangle = \left\langle \mathcal{A}^n(\mathcal{X}), \widehat{v}_h^n(\mathcal{X}) \right\rangle, \tag{4.19}$$

where $\mathcal{X} = \mathcal{X}(\mathbf{x}_j, t_n)$ and the inner products $\langle \cdot, \cdot \rangle$ are defined by

$$\left\langle \widehat{\Theta}_h^n(\mathcal{X}), \widehat{v}_h^n(\mathcal{X}) \right\rangle = \sum_{j=1}^{Ne} \int_{\widehat{\mathcal{K}}_j^n} \widehat{\Theta}_h^n(\mathcal{X}) \widehat{v}_h^n(\mathcal{X})\ d\mathcal{X}, \qquad \left\langle \mathcal{T}^n(\mathcal{X}), \widehat{v}_h^n(\mathcal{X}) \right\rangle = \sum_{j=1}^{Ne} \int_{\widehat{\mathcal{K}}_j^n} \mathcal{T}^n(\mathcal{X}) \widehat{v}_h^n(\mathcal{X}), \tag{4.20}$$

with a similar definition for the solution $\widehat{\alpha}_h^n(\mathcal{X})$. Note that, when the integrals in (4.20) are evaluated exactly one obtains

$$\widehat{\Theta}_h^n(\mathcal{X}) = \sum_{j=1}^{M} \widehat{\mathcal{T}}_j^n \widehat{\phi}_j(\mathcal{X}) \qquad \text{and} \qquad \widehat{\alpha}_h^n(\mathcal{X}) = \sum_{j=1}^{M} \widehat{\mathcal{A}}_j^n \widehat{\phi}_j(\mathcal{X}),$$

and we can therefore define a solution $(\widetilde{\Theta}_h^{n+1}(\mathbf{x}), \widetilde{\alpha}_h^{n+1}(\mathbf{x})) \in V_h \times V_h$ as

$$\widetilde{\Theta}_h^{n+1}(\mathbf{x}) = \sum_{j=1}^{M} \mathcal{T}_j^{n+1} \phi_j(\mathbf{x}) \qquad \text{and} \qquad \widetilde{\alpha}_h^{n+1}(\mathbf{x}) = \sum_{j=1}^{M} \mathcal{A}_j^{n+1} \phi_j(\mathbf{x}),$$

with $\mathcal{T}_j^{n+1} = \widehat{\mathcal{T}}_j^n$ and $\mathcal{A}_j^{n+1} = \widehat{\mathcal{A}}_j^n$ for all $j = 1, \ldots, M$. Note that for $\mathcal{X} = \mathcal{X}(\mathbf{x}_j, t_n)$ we have

$$\widetilde{\Theta}_h^{n+1}(\mathbf{x}) = \widehat{\Theta}_h^n\left(\mathcal{X}(\mathbf{x}_j, t_n)\right) \qquad \text{and} \qquad \widetilde{\alpha}_h^{n+1}(\mathbf{x}) = \widehat{\alpha}_h^n\left(\mathcal{X}(\mathbf{x}_j, t_n)\right).$$

In the current study, we propose a Galerkin-characteristic method where the exact evaluation of the L^2-projection of $(\mathcal{T}^n(\mathcal{X}^n), \mathcal{A}^n(\mathcal{X}^n))$ onto $\widehat{V}_h^n \times \widehat{V}_h^n$ are replaced by an approximate L^2-projection that is both computationally efficient and sufficiently accurate. In our simulations, the integral of an arbitrary function W on the element $\widehat{\mathcal{K}}$ is approximated by the quadrature rule

$$\int_{\widehat{\mathcal{K}}} W(\mathbf{x})\ d\mathbf{x} \approx \frac{3\sqrt{3}R^2}{4} \sum_{g=1}^{Nq} w_g W(x_g, y_g), \tag{4.21}$$

where R denotes the radius of the circle circumscribed by the triangle $\widehat{\mathcal{K}}$, $\mathbf{x}_g = \left(x_g, y_g\right)^\top$ is the quadrature point and w_g is its associated weight. Here, Nq is the total number of quadrature points in the rule, compare for example [35]. In our simulations we consider a quadrature rule with $Nq = 1$ with their corresponding quadrature abscissa and weights listed in Table 4.1.

Note that, the solution $\mathbf{\Theta}^{n+1}(\mathbf{x})$ in (4.19) can be reformulated in a matrix form as

$$\left[\widehat{\mathbf{M}}\right]\left\{\mathbf{\Theta}^{n+1}\right\} = \left\{\widehat{\mathbf{R}}\right\}, \tag{4.22}$$

where $\left[\widehat{\mathbf{M}}\right]$ is the mass matrix, the elements $\widehat{m}_{ij}$ of which are given by $\int_{\widehat{\Omega}_j^n} \widehat{\phi}_j(\mathcal{X})\widehat{\phi}_i(\mathcal{X})\ d\mathcal{X}$, $i, j = 1, \ldots, M$, $\left\{\mathbf{\Theta}^{n+1}\right\} = \left(\Theta_1^{n+1}, \ldots, \Theta_M^{n+1}\right)^\top$ and $\left\{\widehat{\mathbf{R}}\right\} = (\widehat{\mathbf{r}}_1, \ldots, \widehat{\mathbf{r}}_M)^\top$, with $\widehat{\mathbf{r}}_j$ being the right-hand side of (4.19). The formulation of the concentration solution can be performed in a similar manner.

Hence, the Galerkin-characteristic L^2-projection method to approximate the solution $\left\{\widehat{\Theta}_h^n(\mathbf{x}), \widehat{\alpha}_h^n(\mathbf{x})\right\}$ is carried out in the following steps:

1. For each mesh element $\mathcal{K}_j$ generate the quadrature pairs $\left(\mathbf{x}_g, w_g\right)$ using for example the approach (4.21).
2. For each quadrature point calculate the departure point $\mathcal{X}_h(\mathbf{x}_g, t_n)$ using the iteration procedure (4.15).
3. Identify the mesh element $\widehat{\mathcal{K}}_g$ where the departure point $\mathcal{X}_h(\mathbf{x}_g, t_n)$ is located.
4. Evaluate the gridpoint approximations $\widehat{\Theta}_h^n(\mathbf{x})$ and $\widehat{\alpha}_h^n(\mathbf{x})$ by solving the linear system (4.22).

Table 4.1: Coordinates and weights of the nodal points used for the quadrature formula.

Point g	Coordinates (x_g, y_g)	Weight w_g
1	$(0,0)$	$\frac{270}{1200}$
2	$\left(\frac{\sqrt{15}+1}{7}R, 0\right)$	$\frac{155-\sqrt{15}}{1200}$
3	$\left(\frac{-\sqrt{15}+1}{14}R, -\frac{\sqrt{15}+1}{14}\sqrt{3}R\right)$	$\frac{155-\sqrt{15}}{1200}$
4	$\left(\frac{-\sqrt{15}+1}{14}R, \frac{\sqrt{15}+1}{14}\sqrt{3}R\right)$	$\frac{155-\sqrt{15}}{1200}$
5	$\left(-\frac{\sqrt{15}-1}{7}R, 0\right)$	$\frac{155+\sqrt{15}}{1200}$
6	$\left(\frac{\sqrt{15}-1}{14}R, -\frac{\sqrt{15}-1}{14}\sqrt{3}R\right)$	$\frac{155+\sqrt{15}}{1200}$
7	$\left(\frac{\sqrt{15}-1}{14}R, \frac{\sqrt{15}-1}{14}\sqrt{3}R\right)$	$\frac{155+\sqrt{15}}{1200}$

We should mention that in contrast to the conventional Galerkin-characteristic method, the Galerkin-characteristic L^2-projection method calculates the characteristic trajectories for all quadrature points belonging to each triangle in the computational domain. Notice that other quadrature rules can also be applied in our Galerkin-characteristics method without major modifications. To solve the reaction-diffusion terms in (2.7b) we use the Crank-Nicolson scheme for the time integration as

$$\begin{aligned} \frac{\Theta_h^{n+1}-\hat{\Theta}_h^n}{\Delta t} - \frac{1}{2}\nabla^2\Theta_h^{n+1} &= W_Z(\hat{\Theta}_h^n)\phi(\hat{\alpha}_h^n) + \frac{1}{2}\nabla^2\hat{\Theta}_h^n, \\ \frac{\alpha_h^{n+1}-\hat{\alpha}_h^n}{\Delta t} - \frac{1}{2Le}\nabla^2\alpha_h^{n+1} &= W_Z(\hat{\Theta}_h^n)\phi(\hat{\alpha}_h^n) + \frac{1}{2Le}\nabla^2\hat{\alpha}_h^n. \end{aligned} \tag{4.23}$$

Then, multiplying by v_h and integrating by parts, we obtain for all $r_h \in R_h$

$$\begin{aligned} \left(\Theta_h^{n+1}, r_h\right) + \frac{\Delta t}{2}\left(\nabla\Theta_h^{n+1}, \nabla r_h\right) &= \left(\widehat{\Theta}_h^n + \Delta t\; g_h(\widehat{\Theta}_h^n, \widehat{\alpha}_h^n), r_h\right) - \frac{\Delta t}{2}\left(\nabla\widehat{\Theta}_h^n, \nabla r_h\right), \\ \left(\alpha_h^{n+1}, r_h\right) + \frac{\Delta t}{2L_e}\left(\nabla\alpha_h^{n+1}, \nabla r_h\right) &= \left(\widehat{\alpha}_h^n + \Delta t\; g_h(\widehat{\Theta}_h^n, \widehat{\alpha}_h^n), r_h\right) - \frac{\Delta t}{2L_e}\left(\nabla\widehat{\alpha}_h^n, \nabla r_h\right). \end{aligned} \tag{4.24}$$

Thus, in the linear system form, we have

$$\begin{aligned} \left([\mathbf{M}] + \frac{\Delta t}{2}[\mathbf{S}]\right)\mathbf{\Theta}^{n+1} &= [\mathbf{M}]\left(\widehat{\mathbf{\Theta}}^n + \Delta t\; g_h(\widehat{\mathbf{\Theta}}^n, \widehat{\boldsymbol{\alpha}}^n)\right) - \frac{\Delta t}{2}[\mathbf{S}]\,\widehat{\mathbf{\Theta}}^n, \\ \left([\mathbf{M}] + \frac{\Delta t}{2L_e}[\mathbf{S}]\right)\boldsymbol{\alpha}^{n+1} &= [\mathbf{M}]\left(\widehat{\boldsymbol{\alpha}}^n + \Delta t\; g_h(\widehat{\mathbf{\Theta}}^n, \widehat{\boldsymbol{\alpha}}^n)\right) - \frac{\Delta t}{2L_e}[\mathbf{S}]\,\widehat{\boldsymbol{\alpha}}^n, \end{aligned} \tag{4.25}$$

where $\mathbf{\Theta}^{n+1} = \left(\mathcal{T}_1^{n+1}, \dots, \mathcal{T}_M^{n+1}\right)^T$, $\widehat{\mathbf{\Theta}}^n = \left(\widehat{\mathcal{T}}_1^n, \dots, \widehat{\mathcal{T}}_M^n\right)^T$, $\boldsymbol{\alpha}^{n+1} = \left(\mathcal{A}_1^{n+1}, \dots, \mathcal{A}_M^{n+1}\right)^T$ and $\widehat{\boldsymbol{\alpha}}^n = \left(\widehat{\mathcal{A}}_1^n, \dots, \widehat{\mathcal{A}}_M^n\right)^T$. Here, $[\mathbf{M}]$ is the same mass matrix as in (4.22) whose elements are defined by $m_{ij} = \int \phi_j\phi_i \; d\mathbf{x}$ and $[\mathbf{S}]$ is stiffness matrix whose elements are given by $s_{ij} = \int \nabla\phi_j\nabla\phi_i \; d\mathbf{x}$, with $i, j = 1, \dots, M$.

For the existence and uniqueness of the solution of (4.11) and (4.24), we have the following theorem:

Theorem **4.2.** *At each time t_n and for given $\left(\Theta_h^n, \alpha_h^n\right) \in R_h \times R_h$ and $\left(\widehat{\Theta}_h^n, \widehat{\alpha}_h^n\right) \in R_h \times R_h$, the problem* (4.11) *and* (4.24) *has a unique solution $\left(\mathbf{u}_h^{n+1}, p_h^{n+1}, \Theta_h^{n+1}, \alpha_h^{n+1}\right)$ in $\mathbf{S}_h \times Q_h \times R_h \times R_h$ which verifies the following bounds:*

$$\left(1 - \frac{c_{\mathbf{f}}}{2}\right) \left\|\mathbf{u}_h^{n+1}\right\|_{L^2(\Omega)^d}^2 \leq \frac{c_{\mathbf{f}}}{2} \left\|\Theta_h^n\right\|_{L^2(\Omega)^d} + \left\|p_h^{n+1} - \Pi_{k-1} p_h^{n+1}\right\|_{L^2(\Omega)}^2, \tag{4.26a}$$

$$\left\|\Theta_h^{n+1}\right\|_{L^2(\Omega)} - \left\|\widehat{\Theta}_h^n\right\|_{L^2(\Omega)} \leq c_g \Delta t \left(\left\|\widehat{\Theta}_h^n\right\|_{L^2(\Omega)} + \left\|\widehat{\alpha}_h^n\right\|_{L^2(\Omega)}\right), \tag{4.26b}$$

and

$$\left\|\alpha_h^{n+1}\right\|_{L^2(\Omega)} - \left\|\widehat{\alpha}_h^n\right\|_{L^2(\Omega)} \leq c_g \Delta t \left(\left\|\widehat{\Theta}_h^n\right\|_{L^2(\Omega)} + \left\|\widehat{\alpha}_h^n\right\|_{L^2(\Omega)}\right), \tag{4.26c}$$

where $c_{\mathbf{f}}$ and c_g are positive constants independent of h. □

Proof. It is clear that the Darcy problem (4.11) has a unique solution since it satisfies the inf-sup condition (4.10). By testing equations (4.11) with $\mathbf{s}_h = \mathbf{u}_h$ and $q_h = p_h$, and using the Cauchy-Schwarz and Young's inequalities along with Assumption 3.3 on $\mathbf{f}_h$, we immediately derive the bound (4.26a).

Next, knowing $\mathbf{u}_h^n \in \mathbf{S}_h$ and thus $\widehat{\Theta}_h^n$ and $\widehat{\alpha}_h^n$ obtained using the Galerkin-characteristic method, the convection-diffusion equations (4.24) admit also a unique solution $\left(\Theta_h^{n+1}, \alpha_h^{n+1}\right) \in R_h \times R_h$. Therefore, if we take $r_h = \Theta_h^{n+1} + \widehat{\Theta}_h^n$ in (4.24), we obtain

$$\left\|\Theta_h^{n+1}\right\|^2 - \left\|\widehat{\Theta}_h^n\right\|^2 + \frac{\Delta t}{2} \left\|\nabla\left(\Theta_h^{n+1} + \widehat{\Theta}_h^n\right)\right\|^2 \quad = \quad \left(\Delta t g_h\left(\widehat{\Theta}_h^n, \widehat{\alpha}_h^n\right), \Theta_h^{n+1} + \widehat{\Theta}_h^n\right).$$

Then, by using the Cauchy-Schwarz and triangle inequalities along with Assumption 3.3 on the function g_h, we obtain for each time t_n the bound (4.26b). Note that (4.26c) can be derived in the same way by testing the second equation in (4.24) with $r_h = \alpha_h^{n+1} + \widehat{\alpha}_h^n$. ■

5. Convergence and stability of the Galerkin-characteristic unified finite element method

In this section, the focus is on the stability and a priori error estimates in the L^2-norm for to the proposed Galerkin-characteristics unified finite element method. We shall first study the stability and convergence for the velocity and pressure solutions and then, stability and error estimates for the temperature and concentration solutions are demonstrated.

5.1. Stability and error estimates for the velocity and pressure

By virtue of [21, 23], we consider the following necessary hypotheses:

Assumption **5.1.** *The spaces $\mathbf{S}_h$ have the following approximation property: given a function $\mathbf{u} \in H^{k+1}(\Omega)^d$, $k = 1, 2$, there exists $u_h \in \mathbf{S}_h$ such that*

$$\|\mathbf{u} - \mathbf{u}_h\|_{L^2(\Omega)^d} + h\, |\mathbf{u} - \mathbf{u}_h|_{H^1(\Omega)^d} \leq C h^{k+1}\, |\mathbf{u}|_{H^{k+1}(\Omega)^d}, \tag{5.1}$$

where C is a positive constant independent of h.

Assumption **5.2.** *We assume that for all $p \in H^1(\Omega)$, there exists a function $p_h \in Q_h$ such that*

$$\|p - p_h\|_{L^2(\Omega)} \leq C h\, |p|_{H^1(\Omega)}, \tag{5.2}$$

where C is a positive constant independent of h.

Assumption **5.3.** *The operator* Π_{k-1} *defined in* (4.9) *satisfies for all* $p \in L^2(\Omega)$*:*

1. Π_{k-1}*:* $L^2(\Omega) \longrightarrow L^2(\Omega)$ *is continuous and satisfies*

$$\|\Pi_{k-1} p\|_{L^2(\Omega)} \leq C \, \|p\|_{L^2(\Omega)} \, , \tag{5.3}$$

where C is a positive constant.

2. *The properties of* Π_{k-1} *must be augmented by the approximation*

$$\|p - \Pi_{k-1} p\|_{L^2(\Omega)} \leq C' h \, |p|_{H^1(\Omega)} \, , \tag{5.4}$$

where C' *is a positive constant independent of h.*

Let $(\mathbf{u}, p)$ and $(\mathbf{u}_h^n, p_h^n)$ be the solutions of the Darcy problems (4.1a) and (4.11), respectively. We rewrite equations (4.1a) in a compact form as

$$\mathcal{S}(\mathbf{u}^n, p^n; \mathbf{s}, q) = \mathcal{L}_{\mathbf{f}}(\mathbf{s}) \, , \qquad \forall \, (\mathbf{s}, q) \in H_0^1(\Omega) \times L_0^2(\Omega), \tag{5.5}$$

where $\mathcal{S}$ is the bilinear form given by

$$\mathcal{S}(\mathbf{u}^n, p^n; \mathbf{s}, q) = \mathcal{A}(\mathbf{u}^n, \mathbf{s}) - \mathcal{B}(p^n, \mathbf{s}) + \mathcal{B}(q, \mathbf{u}^n) \, .$$

Similarly, we can write (4.11) in the following form

$$\widetilde{\mathcal{S}}\left(\mathbf{u}_h^n, p_h^n; \mathbf{s}_h, q_h\right) = \mathcal{L}_{\mathbf{f}}(\mathbf{s}_h) \, , \qquad \forall \, (\mathbf{s}_h, q_h) \in \mathbf{S}_h \times Q_h, \tag{5.6}$$

where $\widetilde{\mathcal{S}}$ is the bilinear form given by

$$\widetilde{\mathcal{S}}\left(\mathbf{u}_h^n, p_h^n; \mathbf{s}_h, q_h\right) = \mathcal{A}\left(\mathbf{u}_h^n, \mathbf{s}_h\right) - \mathcal{B}\left(p_h^n, \mathbf{s}_h\right) + \mathcal{B}\left(q_h, \mathbf{u}_h^n\right) - \mathcal{D}\left(p_h^n, q_h\right).$$

Using (5.3), we can easily show that $\widetilde{\mathcal{S}}$ is continuous such that

$$\widetilde{\mathcal{S}}\left(\mathbf{u}_h^n, p_h^n; \mathbf{s}_h, q_h\right) \leq C\left(\left|\mathbf{u}_h^n\right|_{H^1(\Omega)^d} + \left\|p_h^n\right\|_{L^2(\Omega)}\right)\left(|\mathbf{s}_h|_{H^1(\Omega)^d} + \|q_h\|_{L^2(\Omega)}\right), \tag{5.7}$$

for all $(\mathbf{u}_h, p_h)$ and $(\mathbf{s}_h, q_h)$ in $\mathbf{S}_h \times Q_h$, where C is a positive constant independent of h. The stability of the variational problem (4.11) is provided by the following theorem, the proof for which can be found in [21]:

Theorem **5.1.** *Let* $(\mathbf{S}_h, Q_h)$ *be the pair of spaces defined in* (4.5)*. Then, there exists a positive constant C whose value is independent of h such that*

$$\sup_{(\mathbf{s}_h, q_h) \in \mathbf{S}_h \times Q_h} \frac{\widetilde{\mathcal{S}}\left(\mathbf{u}_h^n, p_h^n; \mathbf{s}_h, q_h\right)}{|\mathbf{s}_h|_{H^1(\Omega)^d} + \|q_h\|_{L^2(\Omega)}} \geq C\left(|\mathbf{u}_h|_{H^1(\Omega)^d} + \|p_h\|_{L^2(\Omega)}\right), \qquad \forall \, (\mathbf{u}_h, p_h) \in \mathbf{S}_h \times Q_h. \quad \square \tag{5.8}$$

To prove convergence of the stabilized solutions of (5.6), we shall establish the following theorem:

Theorem **5.2.** *Let* $(\mathbf{S}_h, Q_h)$ *be the pair of spaces defined in* (4.5)*, let* $(\mathbf{u}, p) \in \mathbf{H}_0(div, \Omega) \times L_0^2(\Omega)$ *be the solution of the Darcy problem* (4.1a) *and let* $(\mathbf{u}_h, p_h) \in \mathbf{S}_h \times Q_h$ *be the solution of the stabilized mixed problem* (4.11)*, where the operator* Π_{k-1} *defined in* (4.9) *satisfies* (5.3)*. Then, there exists a positive constant C whose value is independent of h such that*

$$\begin{aligned} |\mathbf{u}^n - \mathbf{u}_h^n|_{H^1(\Omega)^d} + \left\|p^n - p_h^n\right\|_{L^2(\Omega)} \quad \leq \quad & C\Bigg(\inf_{\mathbf{w}_h \in \mathbf{S}_h} |\mathbf{u}^n - \mathbf{w}_h^n|_{H^1(\Omega)^d} + \inf_{l_h \in Q_h} \left\|p^n - l_h^n\right\|_{L^2(\Omega)} + \\ & \|p^n - \Pi_{k-1} p^n\|_{L^2(\Omega)} + R_p \left\|\Theta_h^{n-1} - \Theta^{n-1}\right\|_{L^2(\Omega)^d} \Bigg). \quad \square \end{aligned} \tag{5.9}$$

Proof. Since $(\mathbf{S}_h, Q_h)$ is a subspace of $\mathbf{H}_0(div,\Omega)\times L^2_0(\Omega)$, (4.1a) yields

$$\begin{aligned} \mathcal{A}(\mathbf{u}^n,\mathbf{s}_h)-\mathcal{B}(p^n,\mathbf{s}_h) &= \mathcal{L}_{\mathbf{f}}(\mathbf{s}_h), && \forall\, \mathbf{s}_h\in\mathbf{S}_h,\\ \mathcal{B}(q_h,\mathbf{u}^n) &= 0, && \forall\, q_h\in Q_h, \end{aligned} \tag{5.10}$$

where $\mathcal{L}_{\mathbf{f}}(\mathbf{s}_h)=\int_\Omega \mathbf{f}\cdot\mathbf{s}_h\, d\Omega=\int_\Omega R_p\left(\Theta_h^{n-1}-\Theta^{n-1}\right)\mathbf{e}\cdot\mathbf{s}_h\, d\Omega$. Subtracting these equations from (4.11) we obtain

$$\begin{aligned} \mathcal{A}\left(\mathbf{u}_h^n-\mathbf{u}^n,\mathbf{s}_h\right)-\mathcal{B}\left(p_h^n-p^n,\mathbf{s}_h\right) &= \int_\Omega R_p\left(\Theta_h^{n-1}-\Theta^{n-1}\right)\mathbf{e}\cdot\mathbf{s}_h\, d\Omega, && \forall\, \mathbf{s}_h\in\mathbf{S}_h,\\ \mathcal{B}\left(q_h,\mathbf{u}_h^n-\mathbf{u}^n\right) &= \mathcal{D}(p_h,q_h), && \forall\, q_h\in Q_h, \end{aligned} \tag{5.11}$$

or, simply

$$\widetilde{\mathcal{S}}\left(\mathbf{u}_h^n-\mathbf{u}^n,p_h^n-p^n;\mathbf{s}_h,q_h\right)=\int_\Omega R_p\left(\Theta_h^{n-1}-\Theta^{n-1}\right)\mathbf{e}\cdot\mathbf{s}_h\, d\Omega+\mathcal{D}(p^n,q_h), \qquad \forall\,(\mathbf{s}_h,q_h)\in\mathbf{S}_h\times Q_h. \tag{5.12}$$

Let $(\mathbf{w}_h^n,l_h^n)$ be an arbitrary pair in $\mathbf{S}_h\times Q_h$, we shall estimate the discrete error

$$\left|\mathbf{u}_h^n-\mathbf{w}_h^n\right|_{H^1(\Omega)^d}+\left\|p_h^n-l_h^n\right\|_{L^2(\Omega)}. \tag{5.13}$$

Using the inequality (5.8) with (5.12), we obtain

$$\begin{aligned} C\Big(|\mathbf{u}_h^n-\mathbf{w}_h^n|_{H^1(\Omega)^d}+\left\|p_h^n-l_h^n\right\|_{L^2(\Omega)}\Big) &\le \sup_{(\mathbf{s}_h,q_h)\in\,\mathbf{S}_h\times Q_h}\frac{\widetilde{\mathcal{S}}(\mathbf{u}_h^n-\mathbf{w}_h^n,p_h^n-l_h^n;\mathbf{s}_h,q_h)}{|\mathbf{s}_h|_{H^1(\Omega)^d}+\|q_h\|_{L^2(\Omega)}}\\ &= \sup_{(\mathbf{s}_h,q_h)\in\,\mathbf{S}_h\times Q_h}\frac{\widetilde{\mathcal{S}}(\mathbf{u}_h^n-\mathbf{u}^n,p_h^n-p^n;\mathbf{s}_h,q_h)+\widetilde{\mathcal{S}}(\mathbf{u}^n-\mathbf{w}_h^n,p^n-l_h^n;\mathbf{s}_h,q_h)}{|\mathbf{s}_h|_{H^1(\Omega)^d}+\|q_h\|_{L^2(\Omega)}}\\ &\le \sup_{(\mathbf{s}_h,q_h)\in\mathbf{S}_h\times Q_h}\frac{\mathcal{D}(p,q_h)+\int_\Omega R_p(\Theta_h^{n-1}-\Theta^{n-1})\mathbf{e}\cdot\mathbf{s}_h\, d\Omega+\widetilde{\mathcal{S}}(\mathbf{u}^n-\mathbf{w}_h^n,p^n-l_h^n;\mathbf{s}_h,q_h)}{|\mathbf{s}_h|_{H^1(\Omega)^d}+\|q_h\|_{L^2(\Omega)}}. \end{aligned}$$

From (5.7), we have

$$\widetilde{\mathcal{S}}\left(\mathbf{u}^n-\mathbf{w}_h^n,p^n-l_h^n;\mathbf{s}_h,q_h\right)\le C'\left(\left\|\mathbf{u}^n-\mathbf{w}_h^n\right\|_{H^1(\Omega)^d}+\left\|p^n-l_h^n\right\|_{L^2(\Omega)}\right)\left(|\mathbf{s}_h|_{H^1(\Omega)^d}+\|q_h\|_{L^2(\Omega)}\right), \tag{5.14}$$

where C' is a positive constant. Using (5.3), we have

$$\mathcal{D}(p,q_h)\le C''\mathcal{D}(p,p)^{1/2}\,\|q_h\|_{L^2(\Omega)},$$

where C'' is a positive constant. Using the Cauchy-Schwarz inequality and (2.10) we get

$$\int_\Omega R_p\left(\Theta_h^{n-1}-\Theta^{n-1}\right)\mathbf{e}\cdot\mathbf{s}_h\, d\Omega\le R_p\left\|\Theta_h^{n-1}-\Theta^{n-1}\right\|_{L^2(\Omega)^d}\|\mathbf{s}_h\|_{L^2(\Omega)^d}. \tag{5.15}$$

Hence, we obtain

$$\begin{aligned} C\Big(|\mathbf{u}_h^n-\mathbf{w}_h^n|_{H^1(\Omega)^d}+\left\|p_h^n-l_h^n\right\|_{L^2(\Omega)}\Big) \le\; & \sup_{(\mathbf{s}_h,q_h)\in\mathbf{S}_h\times Q_h}\frac{C''\mathcal{D}(p,p)^{1/2}\|q_h\|_{L^2(\Omega)}+R_p\|\Theta_h^{n-1}-\Theta^{n-1}\|_{L^2(\Omega)^d}\|\mathbf{s}_h\|_{L^2(\Omega)^d}}{|\mathbf{s}_h|_{H^1(\Omega)^d}+\|q_h\|_{L^2(\Omega)}}+\\ & \sup_{(\mathbf{s}_h,q_h)\in\mathbf{S}_h\times Q_h}\frac{C'\Big(\|\mathbf{u}^n-\mathbf{w}_h^n\|_{H^1(\Omega)^d}+\|p^n-l_h^n\|_{L^2(\Omega)}\Big)\Big(|\mathbf{s}_h|_{H^1(\Omega)^d}+\|q_h\|_{L^2(\Omega)}\Big)}{|\mathbf{s}_h|_{H^1(\Omega)^d}+\|q_h\|_{L^2(\Omega)}}. \end{aligned}$$

As a result, we get

$$C\Big(|\mathbf{u}_h^n-\mathbf{w}_h^n|_{H^1(\Omega)^d}+\left\|p_h^n-l_h^n\right\|_{L^2(\Omega)}\Big)\le C''\mathcal{D}(p,p)^{1/2}+R_p\|\Theta_h^{n-1}-\Theta^{n-1}\|_{L^2(\Omega)^d}+C'\Big(|\mathbf{u}^n-\mathbf{w}_h^n|_{H^1(\Omega)^d}+\left\|p^n-l_h^n\right\|_{L^2(\Omega)}\Big),$$

or, simply

$$C\Big(|\mathbf{u}_h^n-\mathbf{w}_h^n|_{H^1(\Omega)^d}+\left\|p_h^n-l_h^n\right\|_{L^2(\Omega)}\Big) \leq C''\,\|p^n-\Pi_{k-1}p^n\|_{L^2(\Omega)}+R_p\|\Theta_h^{n-1}-\Theta^{n-1}\|_{L^2(\Omega)^d}+ C'\Big(|\mathbf{u}^n-\mathbf{w}_h^n|_{H^1(\Omega)^d}+\left\|p^n-l_h^n\right\|_{L^2(\Omega)}\Big).$$

Next, we use the triangle inequality to obtain

$$|\mathbf{u}^n-\mathbf{u}_h^n|_{H^1(\Omega)^d}+\left\|p^n-p_h^n\right\|_{L^2(\Omega)}\leq\Big(|\mathbf{u}^n-\mathbf{w}_h^n|_{H^1(\Omega)^d}+\left\|p^n-l_h^n\right\|_{L^2(\Omega)}\Big)+\Big(|\mathbf{u}_h^n-\mathbf{w}_h^n|_{H^1(\Omega)^d}+\left\|p_h^n-l_h^n\right\|_{L^2(\Omega)}\Big).$$

Then,

$$|\mathbf{u}^n-\mathbf{u}_h^n|_{H^1(\Omega)^d}+\left\|p^n-p_h^n\right\|_{L^2(\Omega)} \leq |\mathbf{u}^n-\mathbf{w}_h^n|_{H^1(\Omega)^d}+\left\|p^n-l_h^n\right\|_{L^2(\Omega)}+\frac{1}{C}\Big(C''\,\|p^n-\Pi_{k-1}p^n\|_{L^2(\Omega)}+ R_p\|\Theta_h^{n-1}-\Theta^{n-1}\|_{L^2(\Omega)^d}+C'\Big(|\mathbf{u}^n-\mathbf{w}_h^n|_{H^1(\Omega)^d}+\left\|p^n-l_h^n\right\|_{L^2(\Omega)}\Big),$$

Thus, we can easily deduce by taking the maximum of C, C' and C'' that there exists a positive constant such that

$$|\mathbf{u}^n-\mathbf{u}_h^n|_{H^1(\Omega)^d}+\left\|p^n-p_h^n\right\|_{L^2(\Omega)} \leq C\Big(|\mathbf{u}^n-\mathbf{w}_h^n|_{H^1(\Omega)^d}+\left\|p^n-l_h^n\right\|_{L^2(\Omega)}+\|p^n-\Pi_{k-1}p^n\|_{L^2(\Omega)}+ R_p\|\Theta_h^{n-1}-\Theta^{n-1}\|_{L^2(\Omega)^d}\Big).$$

By taking the infimum over $\mathbf{w}^h\in\mathbf{S}_h$ and $l^h\in Q_h$, we obtain (5.9). ■

Note that Theorem 5.2 can be used to show that solutions of the stabilized Darcy problem converge optimally with respect to the regularized solution. From Theorem 5.2, we also deduce the following result for the error estimates of the velocity and pressure solutions.

Lemma **5.1.** *Let $(\mathbf{u},p)$ be the solution of* (4.1a) *and $(\mathbf{u}_h^n,p_h^n)$ be the solution of* (4.11) *at each time step t_n. Under Assumption 5.1, Assumption 5.2 and Assumption 5.3, there exists a positive constant C depending on $\mathbf{u}$ and p such that*

$$|\mathbf{u}^n-\mathbf{u}_h^n|_{H^1(\Omega)^d}+\left\|p^n-p_h^n\right\|_{L^2(\Omega)}\leq C\Big(h|\mathbf{u}^n|_{H^2(\Omega)^d}+h|p^n|_{H^1(\Omega)^d}+R_p\|\Theta_h^{n-1}-\Theta^{n-1}\|_{L^2(\Omega)^d}\Big).\quad\square \tag{5.16}$$

Proof. Under Assumption 5.1, Assumption 5.2 and Assumption 5.3 and by taking into account the inequality (5.9) of Theorem 5.2, we immediately obtain (5.16). ■

5.2. *Stability and error estimate for temperature and concentration*

Following [15, 36], we consider the one-step method for the computation of the approximate solutions $\{\mathcal{X}_h^n\}$ of (4.12) which has the following form

$$\mathcal{X}_h^n(\mathbf{x})=\mathbf{x}-\Delta t\Phi_{\mathbf{u}_h}(t_{n+1},\mathbf{x},\Delta t),\qquad\forall\,\mathbf{x}\in\Omega_h, \tag{5.17}$$

with $\Phi_{\mathbf{u}_h}(t_{n+1},\mathbf{x},\Delta t)$ being the incremental function. We also consider the following assumptions:

Assumption **5.4.** *We impose the following assumptions:*

1. *There exists a real constant $0<\Delta t_0<1$ such that:*

$$\Phi_{\mathbf{u}_h}:[0,T]\times\Omega_h\times(0,\Delta t_0)\longrightarrow\mathbb{R}^d,$$

is a continuous function that only depends on $\mathbf{u}_h$.

2. *For any $t\in[0,T]$ and $\mathbf{x}\in\Omega_h$, $\Phi_{\mathbf{u}_h}(t,\mathbf{x},\Delta t)\longrightarrow\mathbf{u}_h(\mathbf{x},t)$ as $\Delta t\longrightarrow 0$.*

3. *For any $t \in [0, T]$, $\mathbf{x}, \mathbf{y} \in \Omega_h$ and $\Delta t \in (0, \Delta t_0)$, there exists a positive constant C such that*

$$\left|\Phi_{\mathbf{u}_h}(t, \mathbf{x}, \Delta t) - \Phi_{\mathbf{u}_h}(t, \mathbf{y}, \Delta t)\right| \leq C|\mathbf{x} - \mathbf{y}|.$$

4. *There exists Δt^*, with $0 < \Delta t^* < \Delta t_0$, such that for $\Delta t \in (0, \Delta t^*)$ and $h \in (0, h_0)$, the method is absolutely stable.*
5. *The method is of order p, where p is an integer larger than 0. This means that, if*

$$\mathcal{X}_h(\mathbf{x}, t_{n+1}; t_n) = \mathbf{x} - \int_{t_n}^{t_{n+1}} \mathbf{u}_h\left(t, \mathcal{X}_h(\mathbf{x}, t_{n+1}; t)\right) dt,$$

is the exact solution of (4.12) for any $\mathbf{x} \in \Omega_h$, and we assume that $\mathbf{u}_h(\mathbf{x}, t)$ is sufficiently smooth in time, then for all $\Delta t \in (0, \Delta t^*)$, $h \in (0, h_0)$ and $t_n \in (0, T]$, we have

$$\left|\mathcal{X}_h(\mathbf{x}, t_{n+1}; t_n) - \mathcal{X}_h^n(\mathbf{x})\right| = O(\Delta t^{p+1}).$$

Notice that Assumption 5.4 provide the convergence of $\mathcal{X}_h^n(\mathbf{x})$ to $\mathcal{X}_h(\mathbf{x}, t_{n+1}; t_n)$. We recall the following result concerning convergence of the characteristics:

Lemma **5.1.** *Assume that for each time subinterval $[t_n, t_{n+1}]$, the points $\{\mathcal{X}_h^n(\mathbf{x})\}$ are calculated by the one-step method (5.17) such that Assumptions 5.4 hold. Then*

$$\left\|\mathcal{X}(\mathbf{x}, t_{n+1}; t_n) - \mathcal{X}_h^n(\mathbf{x})\right\|_{L^\infty(0,T;L^2(\Omega))} \leq C\Delta t \, \|\mathbf{u} - \mathbf{u}_h\|_{L^\infty(0,T;L^2(\Omega))} + O(\Delta t^{p+1}), \tag{5.18}$$

where C is a positive constant defined by $C = e^{\Delta t^* |\nabla \mathbf{u}|_{L^\infty(0,T,\Omega)}}$. □

In this instance, it is necessary to impose a condition on Δt to approximate the departure points $\{\mathcal{X}_h^n(\mathbf{x})\}$, under which the functional iterative $\mathbf{d}_{hj}$ defined in (4.14) converges.

Lemma **5.2.** *Suppose that Assumption 3.1 holds and that for all n*

$$\Delta t \|\nabla \Theta_h^n\|_{L^\infty(\Omega)} < 2 \quad \textit{and} \quad \Delta t \|\nabla \alpha_h^n\|_{L^\infty(\Omega)} < 2. \tag{5.19}$$

Then, (5.18) represents an estimate of the committed error to compute the departure points $\{\mathcal{X}_h^n(\mathbf{x})\}$. □

Note that the proofs for Lemma 5.1 and Lemma 5.2 can be found in [15, 36] and are omitted here. As a consequence of the above stability and consistency results for the velocity and pressure solutions and assuming that the method used to compute the departure points points $\mathcal{X}_h$ is stable, we shall study stability and convergence for the temperature and concentration solutions in the L^2-norm. For this purpose, it is convenient to recall the following result of reference [15] (Lemma 6 in page 40) concerning the stability of the Galerkin-characteristic step:

Lemma **5.3.** *Assume that Assumption 5.4 holds, then for any $t_n \in [0, T]$, we have*

$$\|\widehat{\Theta}_h^n\|_{L^2(\Omega)} \leq \|\Theta_h^n\|_{L^2(\Omega)} \qquad \textit{and} \qquad \|\widehat{\alpha}_h^n\|_{L^2(\Omega)} \leq \|\alpha_h^n\|_{L^2(\Omega)}. \; \square \tag{5.20}$$

Next, to prove the convergence of stabilized solutions of (4.24), we shall establish the following theorem:

Theorem **5.3.** *Assume that Assumption 5.4 holds, then for any $t_n \in [0, T]$ we have*

$$\|\Theta_h^{n+1}\|_{L^2(\Omega)} - \|\Theta_h^n\|_{L^2(\Omega)} \leq c_g \Delta t \Big(\|\Theta_h^n\|_{L^2(\Omega)} + \|\alpha_h^n\|_{L^2(\Omega)} \Big), \tag{5.21}$$

and

$$\|\alpha_h^{n+1}\|_{L^2(\Omega)} - \|\alpha_h^n\|_{L^2(\Omega)} \leq c_g \Delta t \Big(\|\Theta_h^n\|_{L^2(\Omega)} + \|\alpha_h^n\|_{L^2(\Omega)} \Big), \tag{5.22}$$

where c_g is a positive constant independent of h. □

Proof. We shall only prove (5.21) since (5.22) can be proved in the same way. If we take $r_h = \Theta_h^{n+1} + \widehat{\Theta}_h^n$ in (4.24), we obtain

$$\|\Theta_h^{n+1}\|^2 - \|\widehat{\Theta}_h^n\|^2 \leq \Big(\Delta t g_h(\widehat{\Theta}_h^n, \widehat{\alpha}_h^n), \Theta_h^{n+1} + \widehat{\Theta}_h^n\Big).$$

Then, using the Cauchy-Schwarz and triangle inequalities along with (5.20) and Assumption 3.3 on the function g_h, we immediately obtain (5.21) for each time step t_n.

■

Next, we proceed to the analysis of the convergence of the proposed method for solving the convection-diffusion equations. For the temperature solution, we consider the standard estimates of $\Theta - P_0\Theta$ and $\Theta - R\Theta$ where P_0 and R are the orthogonal projection and Ritz operators defined in (3.2) and (3.7), respectively. The following estimates hold (see [15] for the proof):

Lemma 5.4. *If w belongs to $L^\infty(0,T;H^r(\Omega))$. Then, for all $t \in [0,T]$, there exist positive constants C_1 and C_2 such that for $1 \leq r \leq m+1$, the temperature solution Θ of* (2.7b) *satisfies*

$$\|\Theta - P_0\Theta\|_{L^\infty(0,T;L^2(\Omega))} + h\ \|\Theta - P_0\Theta\|_{L^\infty(0,T;H^1(\Omega))} \leq C_2 h^r\ \|\Theta\|_{L^\infty(0,T;H^r(\Omega))}, \tag{5.23}$$

and

$$\|\Theta - R\Theta\|_{L^\infty(0,T;L^2(\Omega))} + h\ \|\Theta - R\Theta\|_{L^\infty(0,T;H^1(\Omega))} \leq C_1 h^r\ \|\Theta\|_{L^\infty(0,T;H^r(\Omega))}. \tag{5.24}$$

■

We also recall the following auxiliary results concerning properties of the two mappings $\mathbf{x} \longrightarrow \mathcal{X}(\mathbf{x}, s, t)$ and $\mathbf{x} \longrightarrow \mathcal{X}_h(\mathbf{x}, s, t)$ whose proofs can be found in [37].

Lemma 5.5. *Suppose that Assumption 5.4 holds, then the mapping $\mathbf{x} \longrightarrow \mathcal{X}_h(\mathbf{x}, s; t)$ is a quasi-isometric homeomorphism of Ω into itself with an a.e zero Jacobian determinant.*

■

Another interesting result related with homeomorphisms of the previous results is presented in the following Lemma [38]:

Lemma 5.6. *Let $\mathcal{X}(\mathbf{x}, s; t)$ be the unique solution of* (4.12) *and assume that a quasi-isometric homeomorphism $\mathbf{x} \longrightarrow \mathcal{X}(\mathbf{x}, s; t)$ is of class $C^{r-1,1}(\bar{\Omega})$, $r \geq 1$. Let $f \in W^{r,p}(\bar{\Omega})$ and $h = f(\mathcal{X}(\mathbf{x}, s; t))$, then $h \in \mathbf{W}^{r,p}(\bar{\Omega})$ and there exist positive constants C_1 and C_2 such that*

$$C_1\|f\|_{r,p} \leq \|h\|_{r,p} \leq C_2\|f\|_{r,p}.$$

■

Hence, since $\mathbf{x} \longrightarrow \mathcal{X}(\mathbf{x}, s; t)$ defines a quasi-isometric homeomorphism of Ω onto itself, we can introduce at each time $\sigma \in [t_n, t_{n+1}]$ the ephemeral Ritz projection and L^2-projection operators $R\widehat{\Theta}$ and $P_0\widehat{\Theta}$ as follows:

$$\begin{aligned} R\widehat{\Theta}(\mathbf{x},\sigma) &= z(\mathbf{x},\sigma) = \sum_{j=1}^{M} z_j(\sigma)\phi_j(\mathbf{x}), \\ P_0\widehat{\Theta}(\mathbf{x},\sigma) &= \sum_{j=1}^{M} P_0\widehat{\Theta}_j(\sigma)\phi_j(\mathbf{x}), \end{aligned} \tag{5.25}$$

such that $\forall\ \phi_h \in V_h$

$$\begin{aligned} (\ \nabla z(\mathbf{x},\sigma), \nabla\phi_h) &= \Big(\ \nabla\widehat{\Theta}(\mathbf{x},\sigma), \nabla\phi_h\Big) = P_0\left(g(\mathcal{X}^\sigma,\sigma) - \frac{D\Theta(\mathcal{X}^\sigma,\sigma)}{D\sigma}\right), \\ \Big(P_0\widehat{\Theta}(\mathbf{x},\sigma), \phi_h\Big) &= \Big(\widehat{\Theta}(\mathbf{x},\sigma), \phi_h\Big), \end{aligned} \tag{5.26}$$

where $\widehat{\Theta}(\mathbf{x},\sigma) = \Theta(\mathcal{X}^\sigma,\sigma)$ with $\mathcal{X}^\sigma = \mathcal{X}(\mathbf{x}, t_{n+1}; \sigma)$. By using equation (5.2), it follows that

$$A_h\, z = P_0\left(g(\mathcal{X}^\sigma,\sigma) - \frac{D\Theta(\mathcal{X}^\sigma,\sigma)}{D\sigma}\right), \tag{5.27}$$

where P_0 and A_h are the orthogonal projection and discrete operators defined in (3.2) and (3.6), respectively. Consequently, for $t = t_{n+1}$, $z^{n+1} = R\Theta^{n+1}$ and $\Theta^{n+1} = P_0\Theta^{n+1}$ for all n, and by virtue of Lemma 5.4 and Lemma 5.6, we have the following results [15]:

Lemma **5.7.** *Assume that $\Theta \in L^\infty(0,T;H^{m+1})$. Then, for all $\sigma \in [t_n, t_{n+1}]$ there exist positive constants C_1 and C_2 such that*

$$\|\widehat{\Theta} - z\|_{L^2(\Omega)} + h\|\widehat{\Theta} - z\|_{H^1(\Omega)} \le C_1 h^{m+1}\|\Theta\|_{H^{m+1}(\Omega)},$$

and

$$\|\widehat{\Theta} - P_0\widehat{\Theta}\| \le C_2 h^{m+1}\|\Theta\|_{H^{m+1}(\Omega)}.$$

■

Next, by combining (2.7b) and (5.27), we obtain

$$\frac{\partial z}{\partial\sigma} + A_h z = P_0\left(g(\mathcal{X}^\sigma,\sigma) + \frac{\partial z}{\partial\sigma} - \frac{D\Theta(\mathcal{X}^\sigma,\sigma)}{D\sigma}\right). \tag{5.28}$$

Note that each term of (5.28) is an element of V_h. Now, we discretize (5.28) by the Crank-Nicolson scheme as follows

$$\begin{aligned} z^{n+1} &= E_h z^n + \frac{\Delta t}{2} S_h\left(P_0 g^{n+1} + P_0\widehat{g}^n\right) + S_h P_0\left(z^{n+1} - z^n\right) - \Delta t S_h P_0\left(\frac{D\Theta(\mathcal{X}^{\sigma'},\sigma')}{D\sigma}\right), \\ &\equiv A_1 + A_2 + A_3 + A_4, \end{aligned} \tag{5.29}$$

where $\sigma' = t_n + \dfrac{\Delta t}{2}$ and the operators $E_h : V_h \longrightarrow V_h$ and $S_h : V_h \longrightarrow V_h$ are given by

$$E_h v_h = \left(\frac{I_h - \frac{\Delta t}{2}A_h}{I_h + \frac{\Delta t}{2}A_h}\right)v_h, \qquad S_h v_h = \left(\frac{I_h}{I_h + \frac{\Delta t}{2}A_h}\right)v_h,$$

where $I_h : V_h \longrightarrow V_h$ is the identity operator and E_h and S_h verify $|||E_h||| < 1$ and $|||S_h||| < 1$, with $|||\cdot|||$ being the operator norm. It should be stressed that, for the concentration solution, similar estimates of $\alpha - R\alpha$ and $\alpha - P_0\alpha$ can be obtained using the same steps. Hence, we have the following result for the convergence of the temperature and concentration solutions in the L^2-norm:

Theorem **5.4.** *Assume that the following hypotheses hold:*

1. *$h = O(\Delta t)$,*
2. *Assumption 3.1,*
3. *Assumption 5.4,*
4. *The time step Δt satisfies the condition (5.19).*

Then, there exist positive constants C and C' such that

$$\begin{aligned} \max_{0\le t_n\le T}\left\|\Theta(t_n) - \Theta_h^n\right\| \le\;& C h^{m+1}\|\Theta\|_{L^\infty(0,T;H^{m+1}(\Omega))} + C\left(\frac{h^{m+1}}{\Delta t} + \max_{t\in(0,T)}\beta(t)h^{m+1} + O(\Delta t^p)\right)\|\Theta\|_{L^\infty(0,T;W^{m+1,\infty}(\Omega))} + \\ & C h^{m+1}\|\Theta_t\|_{L^2(0,T;H^{m+1}(\Omega))} + C\Delta t^2\left\|\frac{D^3\Theta}{Dt^3}\right\|_{L^2(0,T;L^2(\Omega))}, \end{aligned} \tag{5.30}$$

and

$$\begin{aligned} \max_{0\le t_n\le T}\left\|\alpha(t_n) - \alpha_h^n\right\| \le\;& C' h^{m+1}\|\alpha\|_{L^\infty(0,T;H^{m+1}(\Omega))} + C'\left(\frac{h^{m+1}}{\Delta t} + \max_{t\in(0,T)}\beta(t)h^{m+1} + O(\Delta t^p)\right)\|\alpha\|_{L^\infty(0,T;W^{m+1,\infty}(\Omega))} + \\ & C' h^{m+1}\|\alpha_t\|_{L^2(0,T;H^{m+1}(\Omega))} + C'\Delta t^2\left\|\frac{D^3\alpha}{Dt^3}\right\|_{L^2(0,T;L^2(\Omega))}, \end{aligned} \tag{5.31}$$

where $\beta(t) = Ke^{Kt}\tau^{\frac{1-m}{2}}(t)$, with $\tau(t) = \min(t,1)$ and K being a constant that depend on the velocity $\mathbf{u}$. □

Proof. We shall prove only (5.30) since (5.32) can be proved in a similar way. Hence, we set

$$\begin{aligned} \Theta^{n+1} - \Theta_h^{n+1} &= (\Theta^{n+1} - z^{n+1}) + (z^{n+1} - \Theta_h^{n+1}), \\ &\equiv \rho^{n+1} + \xi^{n+1}. \end{aligned} \tag{5.32}$$

To estimate ρ^{n+1}, we use $z^{n+1} = R\Theta^{n+1}$ according to (5.25). Next, from Lemma 5.4 it follows that

$$\|\rho^{n+1}\| \le Ch^{m+1}\|\Theta(t_{n+1})\|_{m+1}, \quad \forall\ t_{n+1} \in [0, T]. \tag{5.33}$$

To estimate ξ^{n+1}, we introduce $\bar{z}^n$ that is obtained from Rz^n, then from (5.29) it follows that

$$z^{n+1} = E_h\bar{z}^n + E_h(z^n - \bar{z}^n) + A_2 + A_3 + A_4.$$

Next, taking into account the definition of ξ, we obtain from (4.24) and (5.29) along with $\phi \in V_h$,

$$\begin{aligned} \xi^{n+1} &= E_h\bar{\xi}^n + E_h(z^n - \bar{z}^n) + S_h P_0\Big((z^{n+1} - \Theta^{n+1}) - (z^n - \Theta^n(X_h^n))\Big) + \\ &\quad \Delta t S_h P_0\left(\frac{\Theta^{n+1} - \Theta^n(X^n)}{\Delta t} - \frac{D\Theta}{D\sigma}\Big|_{\sigma=\sigma'}\right) + S_h P_0\Big(\Theta^n(X^n) - \Theta^n(X_h^n)\Big), \\ &\equiv B_1 + B_2 + B_3 + B_4 + B_5, \end{aligned} \tag{5.34}$$

where $\bar{\xi}^n = \bar{z}^n - \Theta_h^{*n}$ is obtained from ξ^n. Now, we estimate the B_i's terms in the L^2-norm.

Estimate of B_1:

From (5.20) and the definition of E_h, we have

$$\|B_1\| \le \||E_h\|| \|\bar{\xi}^n\| \le \|\xi^n\|.$$

Estimate of B_2:

Since

$$\|B_2\| \le \||E_h\|| \|z^n - \bar{z}^n\|,$$

then, from the definition of E_h and triangle inequality, we have

$$\begin{aligned} \|B_2\| &\le \|\widehat{\Theta}^n - I_m\widehat{\Theta}^n\| + \|z^n - \widehat{\Theta}^n\| + \|I_m\widehat{\Theta}^n - \bar{z}^n\|, \\ &\equiv B_1' + B_2' + B_3', \end{aligned}$$

where I_m is the polynomial interpolant of degree m defined in (3.3). The approximation (3.4) and Lemma 5.4 yield

$$B_1' \le Ch^{m+1}|\Theta(t_n)|_{m+1}, \quad \forall\ t_n \in [0, T].$$

Then, by Lemma 5.7, we have

$$B_2' \le Ch^{m+1}\|\Theta(t_n)\|_{m+1}, \quad \forall\ t_n \in [0, T].$$

To estimate B_3', by using the same arguments as in [15] we obtain:

$$B_3' \le Ch^{m+1}\|\Theta(t_n)\|_{m+1,\infty}, \quad \forall\ t_n \in [0, T].$$

Now, taking into account the B_i' estimates and that $W^{m+1,\infty}(\Omega) \subset H^{m+1}(\Omega)$ and $\|\Theta(t_n)\|_{m+1} \le C\|\Theta(t_n)\|_{m+1,\infty}$, it follows that

$$\|B_2\| \le Ch^{m+1}\|\Theta(t_n)\|_{m+1,\infty}, \quad \forall\ t_n \in [0, T].$$

Estimate of B_3:

We have

$$B_3 = S_h P_0 \int_{t_n}^{t_{n+1}} \frac{\partial\Big(z(\mathbf{x},t) - \Theta(\mathcal{X}_h(\mathbf{x},t_{n+1};t),t)\Big)}{\partial t}\, dt.$$

Since $|||S_h||| < 1$ and $|||P_h|||$ are bounded, we obtain from Lemma 5.7

$$\|B_3\| \le Ch^{m+1}\|\Theta_t\|_{L^2(t_n,t_{n+1};H^{m+1}(\Omega))}.$$

Estimate of B_4:

By expanding in Taylor series the term B_4 along the trajectories $\mathcal{X}_h(\mathbf{x},t_{n+1};t)$ with a remaining integral, we obtain

$$\frac{\Theta^{n+1} - \Theta^n(\mathcal{X}^n)}{\Delta t} - \frac{D\Theta}{D\sigma}\Big(\mathcal{X}(\mathbf{x},t_{n+1};\sigma'),\sigma'\Big) = \frac{1}{4\Delta t}\int_{t_n}^{t_{n+1}} (t-t_n)(t-t_{n+1})\frac{D^3\Theta(\mathcal{X}(\mathbf{x},t_{n+1};t),t)}{D^3 t}\, dt.$$

Next, by definition of S_h and P_h, we obtain

$$\|B_4\|^2 \le C\frac{(\Delta t)^4}{4}\int_{t_n}^{t_{n+1}} \left\|\frac{D^3\Theta(\mathcal{X}(\mathbf{x},t_{n+1};t),t)}{D^3 t}\right\|^2 dt,$$

which leads to

$$\|B_4\| \le C\Delta t^2 \left\|\frac{D^3\Theta}{D^3 t}\right\|_{L^2(t_n,t_{n+1};L^2(\Omega))}.$$

Estimate of B_5:

We have

$$\Theta^n(\mathcal{X}^n) - \Theta^n(\mathcal{X}_h^n) = (\mathcal{X}^n - \mathcal{X}_h^n)\int_0^1 D_{\mathcal{X}}\Theta^n(\mathcal{X}^n(\theta))\, d\theta,$$

where $\mathcal{X}^n(\theta) = \theta\mathcal{X}^n + (1-\theta)\mathcal{X}_h^n$, for $0 < \theta < 1$. By using the definition of S_h, P_0 and from Lemma 5.6, we obtain

$$\|B_5\| \le C\|\mathcal{X}^n - \mathcal{X}_h^n\|\|\Theta\|_{L^\infty(t_n,t_{n+1};H^1(\Omega))},$$

then, by introducing (5.18) in the previous estimate, we have

$$\|B_5\| \le C\Delta t\Big(\|\mathbf{u} - \mathbf{u}_h\|_{L^\infty(0,T;L^2(\Omega))} + O(\Delta t^p)\Big)\|\Theta\|_{L^\infty(t_n,t_{n+1};H^1(\Omega))}. \tag{5.35}$$

Next, referring to [39] and under regularity condition on the exact solution $\mathbf{u}$ and the approximate solution $\mathbf{u}_h$, it follows that

$$\|\mathbf{u} - \mathbf{u}_h\| \le \beta(t)h^{m+1}, \quad \forall\, t \in [0,T], \tag{5.36}$$

where

$$\beta(t) = Ke^{Kt}\tau^{\frac{1-m}{2}}(t), \tag{5.37}$$

with $\tau(t) = \min(t,1)$, and K is a constant that depends on $\mathbf{u}$ around the constant $A > 0$ that verifies the condition $\sup\limits_{[0,T)}\|\nabla\mathbf{u}\| \le A$. Then, by substituting (5.36) in (5.35) we have

$$\|B_5\| \le C\Delta t\Big(\beta(t)h^{m+1} + O(\Delta t^p)\Big)\|\Theta\|_{L^\infty(t_n,t_{n+1};H^1(\Omega))}.$$

By summing the estimates B_i's, we obtain

$$\begin{aligned}\|\xi^{n+1}\| \quad \le \quad & \|\xi^n\| + Ch^{m+1}\|\Theta\|_{m+1,\infty} + C\Delta t\Big(\beta(t)h^{m+1} + O(\Delta t^p)\Big) + \|\Theta\|_{L^\infty(t_n,t_{n+1};H^1(\Omega))} + \\ & Ch^{m+1}\|\Theta_t\|_{L^2(t_n,t_{n+1};H^{m+1}(\Omega))} + C\Delta t^2\left\|\frac{D^3\Theta}{D^3 t}\right\|_{L^2(t_n,t_{n+1};L^2(\Omega))}.\end{aligned}$$

By using the Gronwall's inequality, we have

$$
\begin{aligned}
\|\xi^{n+1}\| \quad \leq \quad & \|\xi^0\| + C\frac{h^{m+1}}{\Delta t}\|\Theta\|_{L^\infty(0,T;W^{m+1,\infty}(\Omega))} + C\Big(\max_{t\in(0,T)}\beta(t)h^{m+1} + O(\Delta t^p)\Big)\|\Theta\|_{L^\infty(0,T;H^1(\Omega))} + \\
& Ch^{m+1}\|\Theta_t\|_{L^2(0,T;H^{m+1}(\Omega))} + C\Delta t^2\left\|\frac{D^3\Theta}{Dt^3}\right\|_{L^2(0,T;L^2(\Omega))}. \qquad (5.38)
\end{aligned}
$$

Hence, taking into account that $\xi^0 = 0$, and using (5.32), (5.33) and (5.38) together with the triangle inequality we obtain (5.30).

■

6. Numerical Results

In this section we present numerical results to examine the performance of the Galerkin-characteristic unified finite element method. We first assess the accuracy of the method for two test example with known analytical solutions for a Darcy problem and coupled system. Then we solve the benchmark problem (2.7a)-(2.9) to illustrate the performance of the method for coupled Darcy and convection-diffusion-reaction equations. All the computations are performed on a sequence of unstructured meshes with different element densities using the P_2 elements for all the variables. The linear systems of algebraic equations are solved using the conjugate gradient solver with incomplete Cholesky decomposition. In addition, all stopping criteria for iterative solvers were set to 10^{-7} which is small enough to guarantee that the algorithm truncation error dominates the total numerical error.

6.1. Accuracy example for a Darcy problem

As a first test example, we present numerical results for the Darcy problem (2.7a) rewritten in a simplified form as

$$
\begin{aligned}
\mathbf{u} + \nabla p &= \mathbf{f}, && \text{in} \quad \Omega,\\
\nabla\cdot\mathbf{u} &= 0, && \text{in} \quad \Omega,\\
\mathbf{u}\cdot\mathbf{n} &= 0, && \text{on} \quad \Gamma,
\end{aligned} \qquad (6.1)
$$

where $\Omega = [0,1]\times[0,1]$ and the source term $\mathbf{f}$ is defined such that the analytical solution of (6.1) is given by

$$
p(x,y) = \sin(\pi x)\sin(\pi y), \qquad \mathbf{u}(x,y) = \begin{pmatrix} -\pi\cos(\pi x)\sin(\pi y) \\ \\ -\pi\sin(\pi x)\cos(\pi y) \end{pmatrix}.
$$

Since the exact solution for the problem (6.1) is available, errors and convergence rates for the unified finite element method can be quantified. In Table 6.1 we summarize the errors and convergence rates computed using the L^2-norm for the pressure p, velocity u and velocity v using structured meshes with different number of elements. It is clear that increasing the number of elements in the simulations results in an increase in the L^2-errors for both pressure and velocity solutions. As expected, using the proposed unified finite element method, a second-order accuracy is achieved in both pressure and velocity solutions of the Darcy problem.

6.2. Accuracy example for a coupled Darcy and transport problem

Next we examine the accuracy of the proposed Galerkin-characteristic unified finite element method for solving a coupled Darcy and transport problem. Thus, the problem statement consists of solving the coupled system

$$
\begin{aligned}
\frac{\partial\Theta}{\partial t} + \mathbf{u}\cdot\nabla\Theta - \nu\nabla^2\Theta &= q, && \text{in} \quad \Omega,\\
\mu\mathbf{u} + \nabla p &= \mathbf{f}, && \text{in} \quad \Omega,\\
\nabla\cdot\mathbf{u} &= 0, && \text{in} \quad \Omega,
\end{aligned} \qquad (6.2)
$$

Table 6.1: L^2-error and convergence rates obtained for the pressure and velocity solutions in the accuracy test example of a Darcy problem.

	Pressure p		Velocity u		Velocity v	
Mesh	L^2-error	rate	L^2-error	rate	L^2-error	rate
32×32	6.291E-07	—	2.321E-04	—	2.322E-04	—
64×64	1.595E-07	1.98	6.007E-05	1.95	6.001E-05	1.95
128×128	3.960E-08	2.01	1.523E-05	1.98	1.521E-05	1.98
256×256	9.764E-09	2.02	3.781E-06	2.01	3.776E-06	2.01

Table 6.2: L^2-error and convergence rates obtained for the pressure, velocity and temperature solutions in the accuracy test example of a coupled Darcy and transport problem at two different times.

	Time $t = 1$							
	Pressure p		Velocity u		Velocity v		Temperature Θ	
Mesh	L^2-error	rate	L^2-error	rate	L^2-error	rate	L^2-error	rate
32×32	6.942E-07	—	3.451E-04	—	3.450E-04	—	5.927E-04	—
64×64	1.797E-07	1.95	9.119E-05	1.92	9.117E-05	1.92	1.502E-04	1.98
128×128	4.619E-08	1.96	2.360E-05	1.95	2.359E-05	1.95	3.781E-05	1.99
256×256	1.155E-08	2.0	5.941E-06	1.98	5.939E-06	1.98	9.387E-06	2.01

	Time $t = 2$							
	Pressure p		Velocity u		Velocity v		Temperature Θ	
Mesh	L^2-error	rate	L^2-error	rate	L^2-error	rate	L^2-error	rate
32×32	8.321E-07	—	3.951E-04	—	3.953E-04	—	8.847E-04	—
64×64	2.154E-07	1.95	1.059E-04	1.90	1.052E-04	1.91	2.289E-04	1.95
128×128	5.536E-08	1.96	2.779E-05	1.93	2.761E-05	1.93	5.843E-05	1.97
256×256	1.403E-08	1.98	7.094E-06	1.97	6.999E-06	1.96	1.481E-05	1.98

subject to the following boundary conditions

$$\begin{aligned} (\Theta \mathbf{u} - \nu \nabla \Theta) \cdot \mathbf{n} &= \Theta_{in} \mathbf{u} \cdot \mathbf{n}, \qquad \text{on} \quad \Gamma_{in}, \\ \nu \nabla \Theta \cdot \mathbf{n} &= 0, \qquad\qquad \text{on} \quad \Gamma_{out}, \end{aligned} \tag{6.3}$$

and initial condition

$$\Theta(x, y, 0) = \Theta_0(x, y), \qquad \text{in} \quad \Omega, \tag{6.4}$$

Table 6.3: Mesh statistics, relative errors and computational times for the test problem of moving thermal fronts in a channel without obstacles.

	# of elements	# of nodes	Error in p	Error in u	CPU time (in minutes)
Mesh A	1566	3283	1.503E-03	6.815E-04	1.45
Mesh B	3098	6377	3.890E-04	1.703E-04	3.65
Mesh C	6216	12733	9.393E-05	3.972E-05	7.83
Mesh D	12430	25211	2.190E-05	8.644E-06	15.01
Mesh E	24933	50470	4.934E-06	1.755E-06	32.52

where the boundary regions Γ_{in} and Γ_{out} are defined as

$$\Gamma_{in} = \Big\{\mathbf{x} \in \Gamma : \quad \mathbf{u} \cdot \mathbf{n} < 0\Big\}, \qquad \Gamma_{out} = \Big\{\mathbf{x} \in \Gamma : \quad \mathbf{u} \cdot \mathbf{n} \geq 0\Big\}.$$

with $\mathbf{n}$ is the unit outward normal vector to Γ. Here, we solve the system (6.2)-(6.4) in the unit square $\Omega = [0, 1]\times[0, 1]$ with $\nu = 10^{-3}$ and $\mu = 0.1$. The source terms $q(x, y, t)$ and $\mathbf{f}(x, y, t)$ are calculated such the exact solution of (6.2)-(6.4) is given by

$$p(x, y, t) = 2\sqrt{\mu}\cos\left(\omega + \frac{x}{2\sqrt{\mu}}\right)\exp\left(\frac{y}{2\sqrt{\mu}}\right), \qquad \Theta(x, y, t) = \Big(\cos(\pi x) + \cos(\pi y)\Big)\frac{t}{\pi},$$

$$\mathbf{u} = \begin{pmatrix} \sin\left(\omega + \dfrac{x}{2\sqrt{\mu}}\right)\exp\left(\dfrac{y}{2\sqrt{\mu}}\right) \\ -\cos\left(\omega + \dfrac{x}{2\sqrt{\mu}}\right)\exp\left(\dfrac{y}{2\sqrt{\mu}}\right) \end{pmatrix},$$

where $\omega = 1.05$. A similar test example has been studied in [40] using a local discontinuous Galerkin finite element method. In our simulations we use a fixed time step $\Delta t = 10^{-3}$ and different structured meshes. The obtained results for the L^2-error and convergence rates at times $t = 1$ and $t = 2$ are summarized in Table 6.2. As in the previous test example, the L^2-error decreases as the mesh is refined from one level to the other for all solution variables. These errors have shown similar trend for both considered instants $t = 1$ and $t = 2$. It is also evident that the proposed Galerkin-characteristic unified finite element method preserves the second-order accuracy for all the solutions. Under the considered conditions, the a second-order accuracy is obtained for the pressure, velocity and temperature solutions.

6.3. Moving fronts around an array of circular obstacles

In this example, we consider a Darcian flow in a channel of height H and length $L = H/4$ with different numbers of circular obstacles regularly placed in the second quarter of the channel as shown in Figure 6.1. The sizes of the obstacles are chosen in a way that the space occupied by them is the same for all cases and the distance between the wall and the obstacles nearest to the wall is always half the distance between the obstacles. Thus, when increasing the number of obstacles, this test case represents a flow problem of systematically increasing geometrical complexity. Similar computational domain has been investigated in [41] using the incompressible Navier-Stokes equations but for squared obstacles. In our computations, we assume no volumetric flow rate source and the mean temperature *i.e.* $q = 0$ and $\Theta_0 = 0$. In addition, the non-dimensionless parameters are fixed to $R_p = 7$, $Z = 10$, $L_e = 0.8$, $\delta = 10^{-8}$ and a fixed time step $\Delta t = 10^{-3}$ is used in our simulations.

First we examine the grid convergence in the proposed Galerkin-characteristic finite element method. To this end, we consider five unstructured meshes with different element densities as depicted Figure 6.2. Their corresponding statistics are listed in Table 6.3 along with the CPU times obtained using Mesh A, Mesh B, Mesh C, Mesh D and

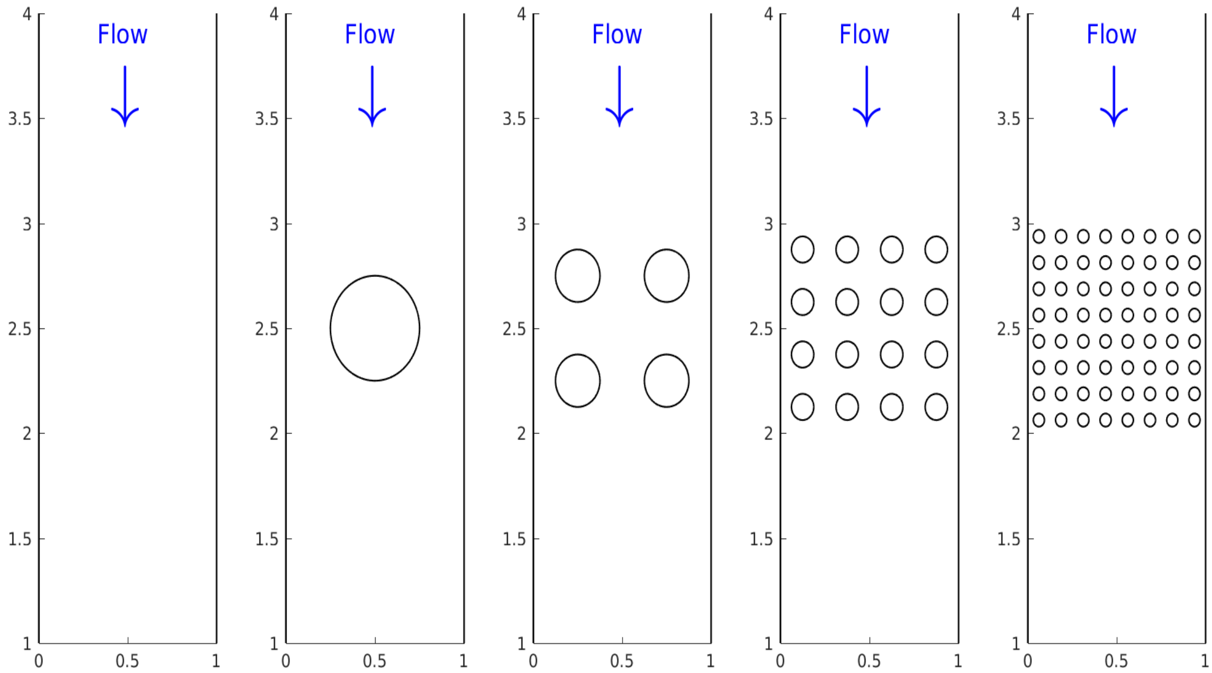

Figure 6.1: Illustration of the geometry used for the problem of moving fronts. An array of circular obstacles is inserted in the channel.

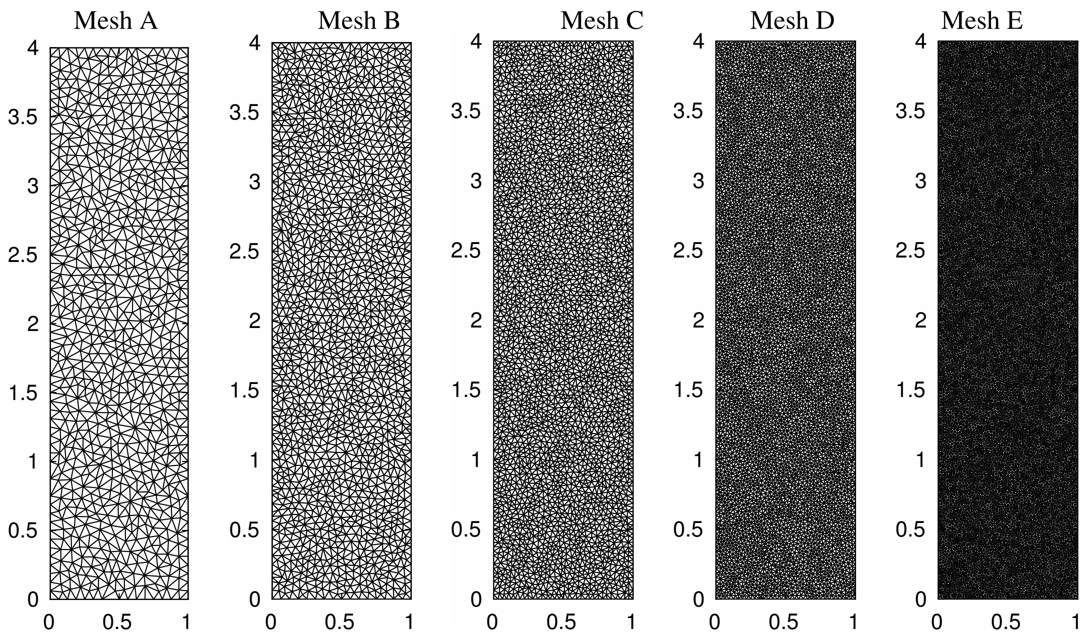

Figure 6.2: Meshes used in the simulations for moving thermal fronts in a channel without obstacles.

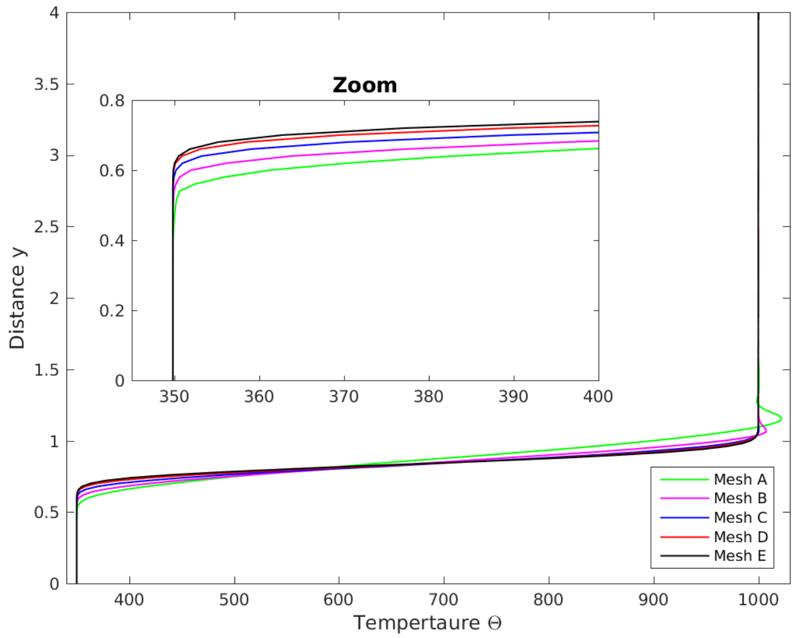

Figure 6.3: Comparison of cross-sections at $x = 0.5$ of the temperature at time $t = 0.2$ using different meshes for the test problem of moving thermal fronts in a channel without obstacles.

Mesh E. A very fine reference mesh with 48392 elements and 109847 nodes is also used in our simulations to quantify errors in the obtained solutions obtained at time $t = 0.2$. As can be seen, for the last two mesh levels Mesh D and Mesh E the differences in errors obtained for the pressure p and velocity u in Table 6.3 are very small. To further qualify the results for these meshes we plot in Figure 6.3 the cross-section results of the temperature obtained using the unified finite element method at the mid-height of the channel $x = 0.5$. It is easy to see that solutions obtained using the Mesh A are far from those obtained by the other meshes. Increasing the density of elements, the results for the Mesh D and Mesh E are roughly similar. Results obtained using the obstacles in the channel and not reported here for brevity, show the same trends. This ensures grid convergence of the numerical results. Hence, the Mesh D is used in all our next computations. The reasons for choosing this mesh structure lie essentially on the computational cost required for each mesh configuration and also on the numerical resolution obtained.

In Figure 6.4 and Figure 6.4, we display the results obtained for the temperature and velocity fields at four different instants namely, $t = 0.05$, $t = 0.1$, $t = 0.15$ and $t = 0.2$.To examine effects of obstacles in the moving thermal front, we present numerical results for the channel without obstacles, with 1×1 cylinder, 2×2 cylinders, 4×4 cylinders and 8×8 cylinders. It is clear that both the temperature patterns and velocity fields are influenced by the inclusion of obstacles in the channel. Increasing the number of cylinders in the computational domain results in a more diffusive thermal front moving downstream. It should be noted that the numerical resolution of computational results have not been deteriorated by the cylinders included in the domain. For instance, the symmetry in these results is fully preserved for all the obstacles accounted for in our simulations. For emphasis these features we illustrate in Figure 6.6 cross-sections of the temperature at $y = 1.75$ obtained in the channel without obstacles and different number of cylinders at time $t = 0.1$. As can be seen from these results, a faster thermal front is detected for simulations without obstacles compared to other simulations with cylinders in the channel. It should be pointed out that the performance of the proposed Galerkin-characteristics unified finite element method is very attractive since the computed solutions remain stable and highly accurate even when coarse meshes are used without requiring nonlinear solvers or small time steps to be taken in the simulations.

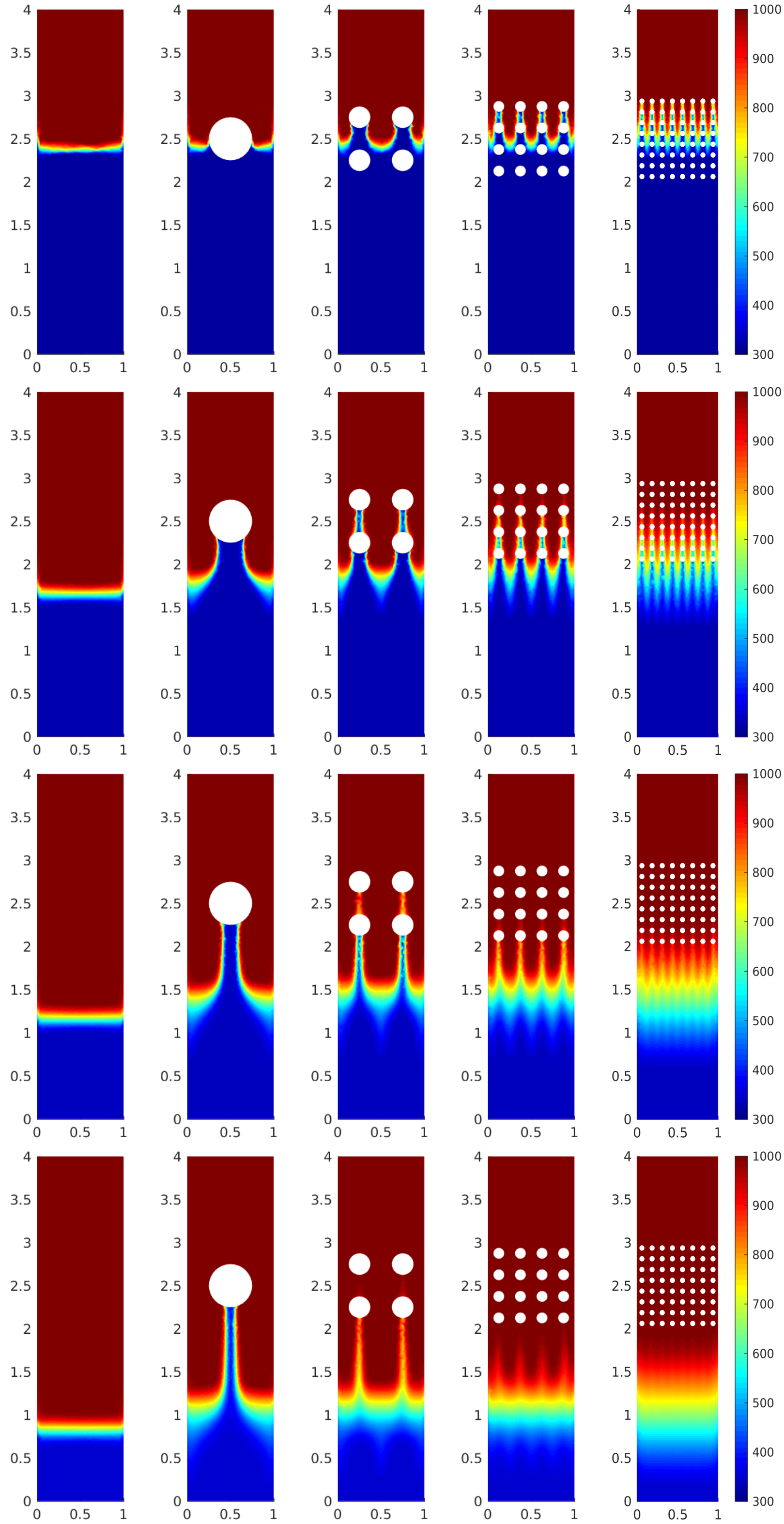

Figure 6.4: Temperature distributions obtained at $t = 0.05$ (first row), $t = 0.1$ (second row), $t = 0.15$ (third row), and $t = 0.2$ (fourth row) obtained in the channel without obstacles (first column), with 1×1 cylinder (second column), 2×2 cylinders (third column) 4×4 cylinders (fourth column) and 8×8 cylinders (fifth column).

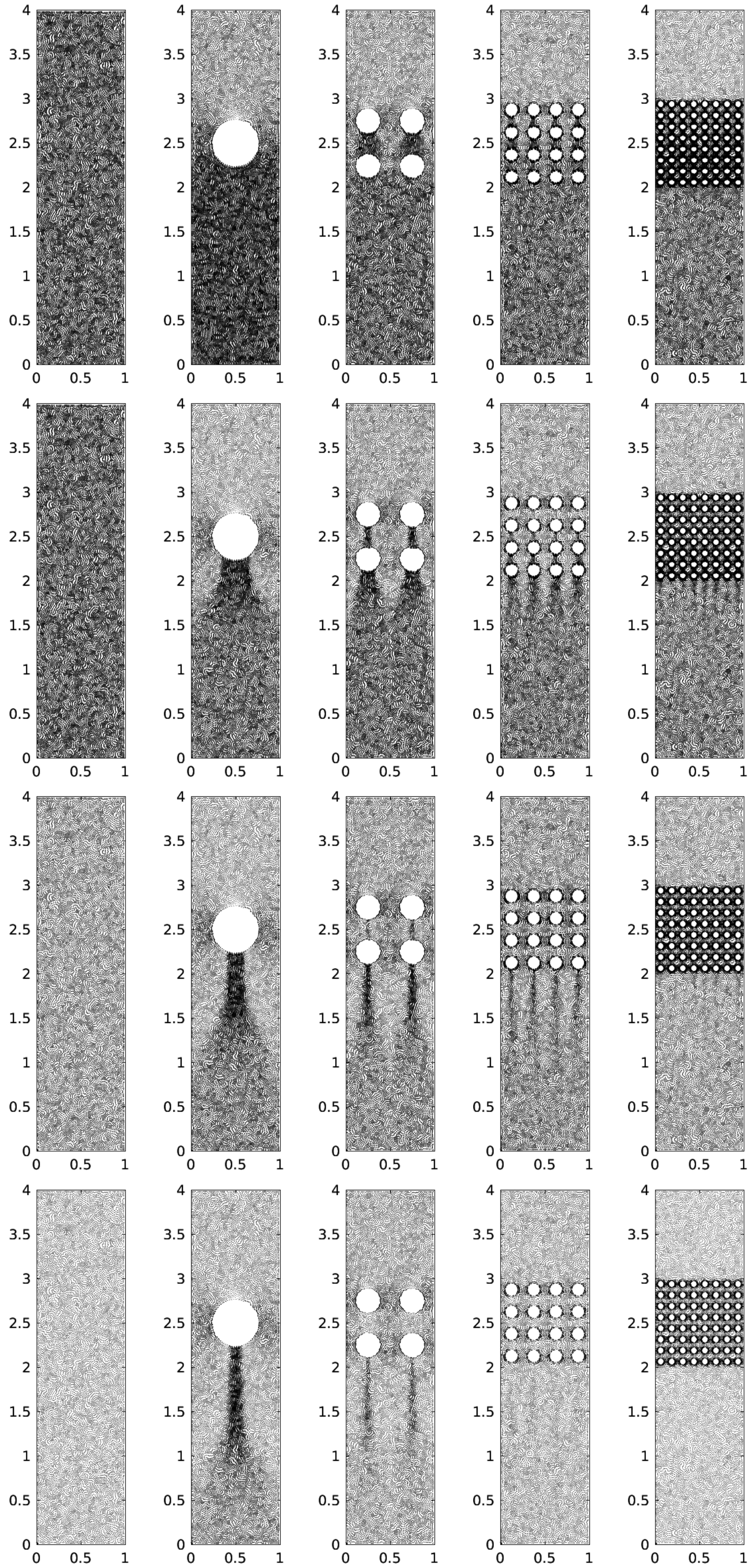

Figure 6.5: Velocity fields obtained at $t = 0.05$ (first row), $t = 0.1$ (second row), $t = 0.15$ (third row), and $t = 0.2$ (fourth row) obtained in the channel without obstacles (first column), with 1×1 cylinder (second column), 2×2 cylinders (third column) 4×4 cylinders (fourth column) and 8×8 cylinders (fifth column).

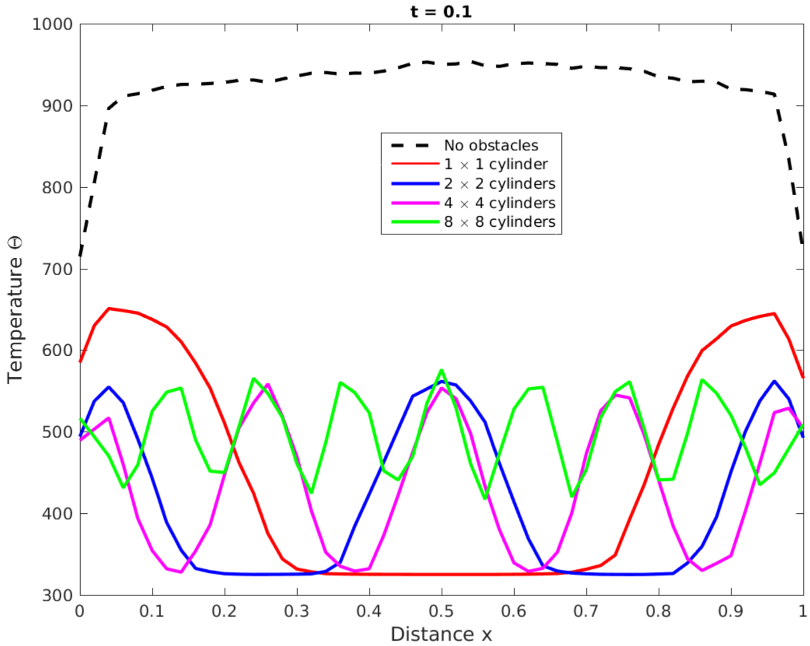

Figure 6.6: Cross-sections of the temperature at $y = 1.75$ obtained in the channel without obstacles and different number of cylinders at time $t = 0.1$.

7. Conclusions

In this study, we have presented a class of unified finite element methods for the numerical simulation of moving thermal fronts in porous media with natural convection. The governing equations consist of the Darcy problem and two convection-diffusion-reaction equations. The coupled system has been integrated using a Galerkin-characteristic finite element method, that combines the semi-Lagrangian method for the time integration with the Galerkin finite element method for the space discretization. A study of stability and convergence have been then carried out and an optimal a priori error estimate has been derived for the numerical scheme used. To improve the accuracy of the approach we have considered an L^2-projection method using an interpolating procedure by tracking the feet of the characteristic lines from the integration nodes. Specific details were given on the implementation of the unified finite element method using unstructured triangular meshes. The main advantage of this method lies on the fact that the pressure and the temperature belong to the same finite element space. The method is stable, accurate, and it can be used to solve both reacting and non-reacting moving thermal fronts. Numerical results have been presented for a test example of moving fronts in a porous media with an array of cylinders. The presented numerical results demonstrate the accuracy of the proposed unified finite element method and its capability to simulate moving fronts in the thermal regimes considered. The effect of increasing the number of cylinders in the flow domain has also been investigated. Future work will concentrate on extension of these techniques to the moving reacting fronts in three-dimensional porous media.

Acknowledgment

Financial support provided by the project CSIC under the contract M MTM2017-89423-P is gratefully acknowledged. The authors would like to thank anonymous referees for giving very helpful comments and suggestions that have greatly improved this paper.

References

References

[1] H. Dejam, M. Hassanzadeh, Diffusive leakage of brine from aquifers during CO_2 geological storage, Advances in Water Resources 111 (2018) 36–57.

[2] R. Gort, J. Brouwers, Theoretical analysis of the propagation of a reaction front in a packed bed, Combustion and flame, Elsevier 124 (2000) 1–13.

[3] S. Yin, A fully coupled finite element framework for thermal fracturing simulation in subsurface cold CO_2 injection, Petroleum 4 (2018) 65–74.

[4] J. Pojman, V. Viner, B. Binici, S. Lavergne, M. Winsper, D. Golovaty, L. Gross, Snell's law of refraction observed in thermal frontal polymerization., Chaos 17 (2007) 033125.

[5] R. P. Washington, O. Steinbock, Frontal free-radical polymerization: Applications to materials synthesis., Polymer News. 28 (2003) 303–310.

[6] E. Bishop, L. Mack, J. Scanlan, Heat transfer by natural convection between concentric spheres, International Journal of Heat and Mass Transfer 9 (1966) 649–662.

[7] D. Oliver, The effect of natural convection on viscous-flow heat transfer in horizontal tubes, Chemical Engineering Science 17 (1962) 335–350.

[8] L. Salhi, H. Rouah, A. Taik, Influence of natural convection on stability of an inclined front propagation, Commun. Fac. Sci. Univ. Ank. Ser. A1 Math. Stat. 68, 1 (2019) 1097–1113.

[9] L. Salhi, A. Taik, Reaction fronts in porous media, influence of Lewis number, linear stability analysis, Int. J. Adv. Appl. Math. and Mech. 5(1), 1 – 13 (2017).

[10] A. Halassi, J. Joundy, L. Salhi, A. Taik, A meshfree method for heat explosion problems with natural convection in inclined porous media, MATEC Web of Conferences 241, 01019 (2018).

[11] S. Chen, W. Gong, Y. Yan, Conjugate natural convection heat transfer in an open-ended square cavity partially filled with porous media, International Journal of Heat and Mass Transfer 124 (2018) 368–380.

[12] J. Lee, Numerical simulation of natural convection in a horizontal enclosure: Part I. on the effect of adiabatic obstacle in middle, International Journal of Heat and Mass Transfer 124 (2018) 220–232.

[13] T. Liu, A. Campbell, A. Hayhurst, S. Cardoso, On the occurrence of thermal explosion in a reacting gas: The effects of natural convection and consumption of reactant, Combustion and Flame 157 (2010) 230–239.

[14] S. Boetcher, Natural convection heat transfer from horizontal cylinders, Thermal Engineering and Applied Science (2014) 1–21.

[15] M. Bermejo, R. El-Amrani, A finite element semi-Lagrangian explicit Runge-Kutta-Chebyshev method for convection dominated reaction-diffusion problems., J. Comp. Applied Math. 154 (2003) 27–61.

[16] M. El-Amrani, M. Seaid, Numerical simulation of natural and mixed convection flows by Galerkin-characteristic method., Int. J. Num. Meth. Fluids. 53 (2007) 1819–1845.

[17] A. Robert, A stable numerical integration scheme for the primitive meteorological equations., Atmos. Ocean. 19 (1981) 35–46.

[18] M. Seaid, Semi-Lagrangian integration schemes for viscous flows., Comp. Methods in App. Math. 4 (2002) 392–409.

[19] A. Temperton, C. Staniforth, An efficient two-time-level semi-Lagrangian semi-implicit integration scheme., Quart. J. Roy. Meteor. Soc. 113 (1987) 1025–1039.

[20] T. Douglas, J. Russell, Numerical methods for convection dominated diffusion problems based on combining the method of characteristics with finite elements or finite differences., SIAM J. Numer. Anal. 19 (1982) 871–885.

[21] P. Bochev, C. Dohrmann, M. Gunzburger, Stabilization of low-order mixed finite elements for the Stokes equations, SIAM Journal on Numerical Analysis 44 (1) (2006) 82–101.

[22] C. Bochev, P.B. Dohrmann, A computational study of stabilized, low-order C^0 finite element approximations of darcy equations., Computational Mechanics. 38 (2006) 223–323.

[23] C. Dohrmann, P. Bochev, A stabilized finite element method for the Stokes problem based on polynomial pressure projections., International Journal for Numerical Methods in Fluids (2004).

[24] K. Allali, A. Ducrot, A. Taik, V. Volpert, Convective instability of reaction fronts in porous media, Math. Model. Nat. Phenom. 2(2) (2007) 20–39.

[25] M. Garbey, A. Taik, V. Volpert, Influence of natural convection on stability of reaction fronts in liquids, Quart. Appl. Math. 53 :1–35 (1998).

[26] H. Rui, J. Zhang, A stabilized mixed finite element method for coupled Stokes and Darcy flows with transport, Computer Methods in Applied Mechanics and Engineering 315 (2017) 169–189.

[27] Y. Amanbek, G. Singh, G. Pencheva, M. Wheeler, Error indicators for incompressible Darcy flow problems using enhanced velocity mixed finite element method, Computer Methods in Applied Mechanics and Engineering 363 (2020) 112884.

[28] F. Brezzi, On existence, uniqueness, and approximation of saddle-point problems arising from Lagrangian multipliers, RAIRO Model. Math. Anal. Numer. 21: 129–151 (1974).

[29] J. Boland, R. A. Nicolaides, Stable and semistable low order finite elements for viscous flows, SIAM J. Numer. Anal. 22 (1985) 474–492.

[30] M. Gunzburger, Finite element methods for viscous incompressible flows, Academic Press, Boston (1989).

[31] O. Pironneau, On the transport-diffusion algorithm and its applications to the Navier-Stokes equations., Numer. Math. 38 (1982) 309–332.

[32] H. Notsu, H. Rui, M. Tabata, Development and L2-analysis of a single-step characteristics finite difference scheme of second order in time for convection-diffusion problems, J. Algorithms Comput. Technol. 7 (2013) 343–380.

[33] H. Notsu, M. Tabata, Error estimates of a pressure-stabilized characteristics finite element scheme for the Oseen equations, J Sci Comput, springer 65 (2015) 940–955.

[34] C. Foicas, C. Guillopé, R. R. Temam, Lagrangian representation of the flow, J. Diff. Eqns 57 (1985) 440–449.

[35] I. Abramowitz, M. Stegun, Handbook of Mathematical Functions with Formulas, Graphs, and Mathematical Tables., Vol. 53, U.S. Department of Commerce., 1972.

[36] M. El-Amrani, M. Seaid, Convergence and stability of finite element modified method of characteristics for the incompressible Navier-Stokes equations., J. Numer. Math. 15 (2007) 101–135.
[37] E. Süli, Convergence and nonlinear stability of the Lagrange-Galerkin method for the Navier-stokes equations., Numer. Math. 53 (1988) 1025–1039.
[38] V. Maz'ya, Sobolev spaces, Springer, 2013.
[39] J. Heywood, R. Rannacher, Finite element approximation of the non-stationary Navier-Stokes problem: Part III, SIAM Journal of Numerical Analysis. 25, 489-512 (1988).
[40] D. Vassilev, I. Yotov, Coupling Stokes-darcy flow with transport, SIAM Journal on Scientific Computing 31(5):3661-3684 (2009).
[41] J. Bernsdorf, F. Durst, M. Schäfer, Comparison of cellular automata and finite volume techniques for simulation of incompressible flows in complex geometries, Int. J. Numer. Meth. Fluids 29 (1999) 251–264.